Melt Electrospinning of Shape Memory Polymer: An Initial Examination of the Morphological, Mechanical and Shape Memory Properties of Non-woven Melt-Electrospun Polyurethane Shape Memory Polymer Mats.

by

Alan David White

A thesis submitted in partial fulfillment of the requirements for the degree of

Master of Science

Department of Mechanical Engineering
University of Alberta

© Alan David White, 2020

Abstract

Shape memory polymers (SMP) are a class of smart materials which are able to memorize a temporary shape and recall their original/permanent shape with the application of a stimulus. The electrospinning process has been utilized to produce fibrous SMP membranes from polymer solutions, but this process has the side effect of introducing toxic solvents into the materials particularly for biomedical applications. The melt-electrospinning process is a fiber production method that utilizes electrostatic forces in order to produce fibers with micro-diameters from a polymer melt. As such, it does not require use of solvents. In this thesis, I describe how the melt-electrospinning process was used to successfully produce fiber mats from polyurethane SMP (SMPU), and investigate the effect of varying the applied voltage and gap distance on the morphological, mechanical and shape memory properties of the non-woven mats.

To examine the effect of varying the applied voltage and gap distance on the properties of the mats, four parameter cases were used to generate SMPU mats on an in-house built melt-electrospinning apparatus. The applied voltage was varied from 15 kV to 20 kV, and the spinning gap was varied from 5 cm to 10 cm in order to create the four cases.

The morphology and fiber diameter of the mats were examined by SEM. It was found that all four cases produced smooth fibers. Over the investigated ranges, the variation of the spinning parameters caused a change in the structural layout of the mats if the change in the electrical field strength caused by the parameter variation was large enough. The diameter of the fibers ranged from 28.4 ± 6.8 μm to 73.6 ± 18.9 μm. Diameter was found to appear to increase when spinning distance was increased at both voltage levels, while diameter appeared to decreased when voltage was varied at a 5 cm gap distance, with no apparent change at a 10 cm gap distance. These apparent

variations are attributed to the change in electrical field strength and thus the force on the polymer melt from increasing the voltage or gap distance respectively.

The mechanical properties of SMPU mats at all four parameter cases were characterized. The Young's modulus and tensile strength ranged from 8.38 ± 2.41 MPa to 14.2 ± 4.0 MPa and 2.13 ± 0.23 MPA to 4.27 ± 0.74 MPa respectively over the four investigated cases. No apparent variation in the Young's modulus was found over the range of parameters investigated. This was attributed to the fiber diameters being above a critical diameter below which a change in diameter would affect the Young's modulus due to polymer chain alignment. For the yield strength, no apparent change was found with varied voltage, but increasing the gap distance resulted in an apparent decrease. This is attributed to the decrease in complexity of mat structure due to decreased electrical field strength, resulting in straighter fibers, which result in the mat fully yielding before a more complex fiber structure would.

Finally, the shape memory properties of the SMPU mats were determined by programming the materials and recovering them in order to determine the recovery ratio and recovery rate of the fibrous mats. The recovery ratio varied from 33.2 ± 2.2 % to 61.9 ± 6.1% with parameter variation. Variation of the applied voltage had no apparent impact on the recovery ratio, while increasing the gap distance produced an apparent decrease at both voltages. This apparent decrease was attributed to larger changes in the electrical field strength, which led to larger changes in the level of polymeric chain alignment in the polymer fibers. The recovery rate was found to vary from 0.00410 ± 0.00062 mm/s to 0.00723 ± 0.00129 mm/s, with the only change being an apparent decrease in the recovery rate when the gap distance was varied from 5 cm to 10 cm at 15 kV. This limited impact was attributed to only this case having a large enough change in electrical field strength / diameter in order to effect the polymer chain entanglement governing the recovery rate.

This work shows that melt-electrospinning is a viable technique for SMPU, and that variation of spinning parameters results in variation of the morphological, mechanical and shape memory properties of the generated materials.

Preface

The Thesis presented here is a wholly original work produced by Alan David White. No portion of the work presented here has been published previously

Dedication

This work is dedicated to my parents, Gary and Victoria White. As I have moved through my educational journey, in both the good and bad times, they have always provided me with the support and encouragement I have needed to keep moving towards my goals, and as such their support has been essential in coming to the completion of this work.

Acknowledgments

I would like to thank my supervisor, Dr. Cagri Ayranci for his guidance and support throughout the production of this work. I would also like to thank my parents, Gary and Victoria, for their unending support over the course of my education.

Table of Contents

List of Tables

List of Figures

Chapter 1 Introduction

This work seeks to investigate melt-electrospinning of shape memory polymer polyurethane. Chapter 1 presents an overview of shape memory polymers, the general electrospinning process, including both solution and melt electrospinning, and the application of the solution electrospinning process of shape memory polymers. As well, applications of both shape memory polymers and electrospun materials are discussed. Chapter 2 presents the systems and materials used in completing the research and data collection upon which this work is based, including detailed descriptions of the melt-electrospinning system utilized in this work and the polyurethane shape memory polymer used. The experimental design is also described in this section. Chapter 3 presents the results of research completed for this thesis, including the morphological analysis, mechanical analysis and shape memory analysis. The reasoning for the results seen in each of these areas are discussed, and possible explanations are presented. Finally, Chapter 4 summarizes the results and major takeaways from the work presented here, and suggests a number of future avenues of potential research to continue growing the understanding of melt-electrospun shape memory polymer.

Shape memory polymers (SMP) are fascinating subgroup of "smart materials" which have the ability to "memorize" a programed shape (temporary shape) and upon external stimulus return to an original, un-deformed shape [1]. A review of the work in shape memory polymers performed by Liu, Qin and Mather [2] states that the first appearance of the shape memory effect with regards to polymers in the literature is a patent from 1941 referencing a dental resin presenting thermal shape memory [2], while Liang, Rogers and Malafeew note that specific shape memory polymers were developed initially in the work of the Nippon Zeon Co. in 1984 [3]. Liu, Qin and Mather also make note of the early use of the shape memory effect with regards to polymers in the development of shrink tubing [2]. Research interest in SMP built up in the mid 1980's particularly with Japanese researchers and this interest grew in the early 1990's with Japanese researches, specifically with a series of papers published by Tobushi, Hayashi, and Kojima focusing on the properties of polyurethane shape memory polymers [4]–[7]. Work performed by Echigo et al. focusing on the use of shape memory polymers in biomedical applications were also published in the early 1990's [8]. Work on shape memory polymers continued in Japan throughout the 1990's largely continuing to focus on polyurethane based SMP (usually referred to as SMPU), with some limited mentions

of other SMP's [9]–[18], with work also starting to be undertaken by researchers outside Japan [3], [19]–[26]. In these early years, of interest in the work on shape memory polymers outside of the Japan, the works of Andreas Lendlein are worth mentioning in the early 2000's [27]. Lendlein's work with SMPs has focused on the use of SMP's in biomedical applications [28]–[30] and the production and characterization of these materials [27], [31], [32], as well as having produced a number of reviews and book chapters on the subject [33], [34]. Following the early work in the 1990's and early 2000's the research interest in SMP has greatly increased. While a Scopus search for the term "shape memory polymer" shows only 50 results from 1986 to 1999, this increases to 572 results between 2000 and 2009, and then to 2862 results between 2010 and 2020 as of April 2020 (Searched on Scopus.com). Based on this increasing trend of publication, it is clear that research interest in SMP materials and their applications is continuing to grow.

While all SMP's share the common ability to memorize a temporary shape and recover an original shape [1], how this recovery is triggered varies depending on the different types of SMPs and their triggering mechanisms. Examples of common activation triggers are heat [3], [8], [25], [28], [29], [35]–[41], and exposure to moisture [42]. Other, more exotic activation methods such as lasers [43], and PH change [44] have also been mentioned in the literature.

SMP materials exist in both the form of thermoset polymers [2], [45] and thermoplastic polymers [2], [45]. In general, in the case of thermally activated SMP's, Liu, Qin and Mather note in their review of the subject that the shape memory effect in polymeric materials can be categorized into four mechanisms [2], with thermoset materials having shape memory effect based on either glassy segments controlling the fixed shape or semi-crystalline segments controlling the fixed shape [2], and thermoplastic materials where the shape memory effect is controlled either by soft segments which soften at a lower temperature than the hard segments making up the polymer [2], or by way of crystallization of the soft segments below a prescribed melting temperature which fixes a programmed shape [2]. Garces et al. note that in particular for thermoplastic polyurethane shape memory polymer that the shape memory effect is due to the phase separated structure of the polymer consisting of both crystalline segments, which serve as hard segments in the polymer, and soft segments, whose lower thermal transition temperature allows for the shape memory effect to take place [45]. This would make these polymers fall under the third category of shape memory

polymers as described by Liu, Qin and Mather, as noted above [2], where the soft segments are programmable/stretchable above their glass transition temperature [2].

SMP's have been utilized in a number of different research areas and applications found in the current literature. Initially, examples of the application based research included biomedical applications [8], [26] and the use of SMP for active disassembly [20], [24]. In the last decade, areas of application research in shape memory polymers include sensing applications [46], space/aerospace applications [47]–[56], self-healing materials [57]–[66], composite materials with SMP as a constituent [67]–[73], biomedical applications [39], [74]–[82], the use of SMP materials for actuation [46], [83]–[87], and the use of SMP in textile applications [88], [89], among others.

Among the possible forms in which SMP can be utilized, fibrous SMP is of major interest for potential applications in biomedical sutures, smart textiles, and the like. One of the most commonly utilized techniques used for the production of fibrous shape memory polymers is the solution electrospinning process. Solution electrospinning is a fiber production process that utilizes a high electrostatic field in order to draw a polymer solution from a spinneret towards a collector [90], during which time the solution solvent evaporates, leaving polymer fiber at the collector [90]. The process is influenced by a number of factors, including the strength of the electric field, the concentration of the polymer solution, the gap distance between the spinneret and the collector, the diameter of the spinneret and the feed rate at which the polymer solution is ejected out of the spinneret [91].

The current available literature presents a number of works which deal with the solution spinning of shape memory polymers. These works show the investigation of a number of different varieties of shape memory polymers being used to generate fibrous materials, including polyurethane SMP's [80], [92]–[103] Poly (Vinyl Acetate) [104], PLA [105] and PDLLA-co-TMC [106], among others. The applications of these generated fibrous materials include the creation of smart cell scaffolds of various types [80], [93], [96], [98], [102], [106]–[109] , the generation of smart fabrics [99], as well as work with regards to generating composites with shape memory characteristics using electrospun polymer [103], [108], [110]–[114]. As well as work with direct applications, studies focused directly on the mechanical and shape memory characteristics of these electrospun materials have also been performed [92], [94], [95], [100], [115]–[117].

While as discussed above, fibrous shape memory polymer materials have been produced through the use of the solution spinning process, this process presents a major issue due to the toxicity of some of the solvents used to produce the polymer solutions [90], common solvents used during solution electrospinning of SMPs being DMF and Toluene. The solvents are not only harmful during the electrospinning process, but also even the small residues of these solvents left on the fibers after the process might pose a health risk particularly for biomedical applications.

In order to bypass this issue this work proposes the use of the melt-electrospinning technique for the production of shape memory polymer fibers, which, to the best knowledge of the author, has not previously been presented in the available literature. Melt-Electrospinning is a relatively young field of enquiry which has grown out of the more robustly examined solution electrospinning approach. It is very similar to the solution electrospinning process previously described, with the only major difference being that the fluid being spun is a pure polymer rather than a polymer in solution with a solvent [90]. Due to this similarity, the parameters governing the process are largely the same, except for the solution concentration parameter being replaced with the temperature of the molten polymer in terms of controlling the viscosity of the spinning medium [118]. The earliest reports of this method in the scientific literature date to the early 1980's, with the publication of three papers by Larrondo and St. John Manley [119]–[121], as noted by Hutmacher and Dalton [122]. They presented work showing the ability to produce polymer fibers from melt by the application of electrostatic force, as was already established for liquids [119]. Following these initial publications, no publications on the subject occurred until 2001 according to a review performed by Hutmacher and Dalton [122]. Following the re-emergence of the melt electrospinning process in academic interest, work has been performed in a number of areas. A major area of investigation has been into the effects of various spinning parameters and polymer parameters on the generated fiber mats [118], [123]–[140]. While this base line study of the process itself has been a focus in the literature, there has also been a focus on applications for the generated material. In general, the applications of melt-electrospun fiber materials have been similar to those of solution spun polymers, including biomedical scaffolding [131], [141]–[146], textile applications [147], as well as filtration [122]. Recently, much of the work relating to melt electrospinning has shifted into the investigation and development of melt electrospinning direct writing methods for various applications [131], [142], [143], [148]–[151]. Due to the pervious use of solution electrospinning to produce shape memory polymer non-wovens, and the general

similarity between this process and the melt-electrospinning process, it is believed that the use of melt-electrospinning for the production of shape memory polymer non-wovens is a possible production method.

As mentioned previously, the majority of the process parameters which effect the melt electrospinning process are shared with the solution electrospinning process. These common parameters include voltage level [122], spinning gap distance [122], the rate at which the polymer is introduced into the electrical field (i.e. feed-rate) [122], and spinneret nozzle diameter [122]. In contrast to the solution electrospinning process, the melt electrospinning process is also effected by the temperature of the molten polymer which is introduced in electric field, which effects the viscosity of the molten polymer and acts as an important parameter for the process [118]. These parameters effect the melt electrospinning system for a number of different reasons. Electrical field strength is the main driving force of the overall process [125], and is effected by both the set voltage level and the gap distance between the spinneret and the collector [133]. The force generated by the induced electrical field causes the polymer melt to overcome its surface tension at the end of the spinneret, forming the Taylor cone and jet which ultimately form the fiber that is collected at the end of the melt electrospinning process [152]. Both the rate at which the polymer is introduced into the electrical field and the spinneret nozzle diameter can be seen to relate to the amount of polymer available to be drawn into fiber at any given time. As stated, the current literature presents a number of studies which have investigated the effects of varying these parameters on the generated polymer fibers [118], [123], [135]–[140], [124]–[126], [128]–[130], [133], [134]. These studies have included investigation into the effect of the process parameters on a number of different aspects of the generated fiber, with many works looking at the effects of the parameters on fiber diameter [118], [124], [138]–[140], [125], [128], [129], [133]–[137], with works also being found looking at the effects of varying the spin parameters on the morphology of the fibers [125], [138], the mechanical properties [133], and amount of degradation caused to the polymer during the spinning process [126]. It should be noted that in general, the process parameters of the melt electrospinning system's effects on the resulting fibers seem to be indifferent to the type of polymer being electro spun in the trends that develop. The electrical field strength is an example of this, with multiple studies utilizing multiple different polymer feed stocks reporting the same effect of increased electrical field strength, namely the decrease in the diameter of the produced polymer fibers [124], [125], [129], [133]–[135], [137]. As noted above, the

electrical field strength is related to both the voltage level that is introduced into the setup via a high voltage source, as well as the spinning gap distance, and that varying either of these parameters will affect the field strength [133]. In particular, increasing the voltage level applied to the system will result in a higher field strength [133], while the same trend can be caused by working with a smaller spinning gap distance [133]. The literature does note some exceptions to this general idea of the effect of the gap distance, with a number of publications noting that while the fiber diameter initially decreased with decreasing gap distance, it was found to begin to increase following a certain critical point [118], [134]. While they did not observe it in their work, Wang and Huang note that they believe that past a critical point, decreasing the gap distance will cease to have the inverse effect on the fiber diameter [133], which agrees with the reversing trend presented above [118], [134]. Deng et al. attribute this effect to the lack of time for the fibers to stretch during the spinning process due to the close proximity to the collection target [134], a conclusion which is concurred with by Yan et. al. [118]. Wang and Huang found that the gap distance also had an effect on the mechanical strength of the generated fiber, with an increased strength coming with decreased gap distance [133], and they attributed this to the decreased fiber diameter [133]. Finally with regards to the gap distance, Dasdemir et al. found that an increased gap distance resulted in a less interconnected mat structure. In terms of the rate at which the polymer was introduced into the electrical field, the literature shows that with increased rate of polymer introduction, the diameter of the generated fibers increased in general [129], [139]. Dalton et al. noted that more fibers did not fully cool and solidify before reaching the collection target with increased rate of polymer introduction [139], and reported a clear increase in the diameter of the collected fibers in the non-solidified state as the rate of polymer introduction was increased [139], but a less direct increase was also seen with regards to the solidified fibers [139], while Doustgani and Ahmadi simply noted an increase in the generated fiber diameter as the polymer introduction rate was raised [129]. Doustgani and Ahmadi attribute this diameter increase simply to the fact that more polymer is available in the system to generate fiber [129]. A similar trend is seen with increasing the inner diameter of the spinneret [118], [134], with a slight exception being noted by Deng et.al, where they found an increase in the diameter of the generated fiber following a decrease of the spinneret diameter to a certain point [134]. They attribute this to the smaller spinneret diameter resulting in higher pressure being required for Taylor cone formation, thus resulting in higher rates of polymer flow [134]. With regards to the temperature/ laser power used

to generate the polymer melt, in general studies found an inverse relationship between the temperature / laser power used to produce the melt and the diameter of the generated fiber [118], [128], [129], [134], [138]. However, similarly to the phenomena described with regards to gap distance, one publication using laser based melting apparatus found that once a certain laser power was reached, the generated fibers began to have increased diameters [138], and a third laser based system found a limit to the effectiveness of increasing the power [128]. Also one work found that for their parameters, the change in spinning temperature did not affect the final diameter of the generated fibers [139]. The temperature / laser power used to generate the fibers was also found to effect the morphology of the generated fibers. Ogata et al. found that when their laser system was set to higher power settings, PET fibers acquired a beaded morphology [140]. It should also be noted that beyond the system process parameters, there are also a number of material specific parameters which have been shown in the literature to effect aspects of fiber generation in melt electrospinning. In particular, the molecular weight of the polymer [129], [135], as well as the tacticity and crystallinity of the polymer being used [136], have been shown to effect the generated fibers.

A number of different polymers have been spun into fibrous materials using the melt electrospinning method, including polyurethane [118], [125], [128], [130], [145], [153], [154], polypropylene [119], [123], [135], [155]–[158], polyethylene [119], [134], PCL [118], [124], [159], [160], [126], [127], [129], [131], [132], [142], [143], [151] and PLA [118], [161]–[163] among others, including blends of various polymers [124], [137], [139], [146], [162], [164]. While the general setup used for melt electrospinning is very similar to the solution electrospinning setup described above, one major difference exists. This major difference, as mentioned previously is that the melt-electrospinning process replaces the dissolved polymer solution with a polymer melt [90]. This change removes the issue of toxicity mentioned previously as a major limitation for the application of solution electrospun materials [90]. A number of different methods are presented in the literature to bring the polymer to the molten state, including the use of electrical resistance heating methods including the use of polymer extruders [119], [125], [148], [153], [155], [156], [165]–[168], [126], [127], [131], [133]–[136], [145] circulating heated fluids [124], [139], [143], [144], [146], [151], [157], [169], the use of heated air [157], oven type systems [123], [147], [158],

[161]–[163], [170], [171] , and the use of laser systems [128], [137], [138], [140], [159], [172]. While the rest of the basic setup for melt electrospinning is relatively constant, a number of different variations do exist. In terms of overall setup, the major possible variation is in either a horizontal [147], [155], [157], [165], [171] or vertical orientation [119], [123], [153], [154]. A final major difference which is found between different melt electrospinning setups is which of the spinneret and collector is grounded and which is charged. While many setups follow the more traditional solution electrospinning paradigm and ground the collection surface [118], [123], [139], [140], [143], [146]–[148], [151], [156], [158], [159], [124], [161]–[164], [168], [170]–[172], [127], [128], [131]–[133], [137], [138], Hutmacher and Dalton make note that when electrical means are used to achieve the molten state, grounding the spinneret may be advantages to avoid electrical interference [122]. This setup is seen in multiple studies where such a configuration is used [126], [133], [165]–[167], [134]–[136], [144], [145], [153]–[155].

To date, no study which focused specifically on the melt-electrospinning of SMP grade polyurethanes and the investigation of the effect of parameters on their shape memory properties has been completed to the best knowledge of the author. This work seeks to investigate the effects of the melt-electrospinning process and the variation of the melt electrospinning parameters on the shape memory properties of MM 4520 shape memory polyurethane, as well as the effect on the morphology and mechanical properties of the same material. This initial investigation will help to show the feasibility of melt-electrospinning SMPU, and the initial characterization of the generated materials will allow for future work to be performed in both applications and further characterization. As well, this advance will open the door to easier and safer biomedical application of non-woven SMPU mats, due to the lack of toxic solvents used in the process versus the current solution electrospun materials [90]. In addition, as the field of melt-electrospinning is still developing, this work will produce additional understanding of the effects of the variation of the spinning parameters in general melt-electrospinning application, allowing for an increase in understanding of the melt-electrospinning process as a whole.

Chapter 2 Materials and Methods

2.1 Materials

MM 4520 shape memory polymer produced by SMP Technologies Inc. (Tokyo, Japan) was the material used in this investigation. The material was received in pellet form from the manufacturer, and was converted into 1.75 mm filament using a Brabender® extruder produced by Brabender® GmbH & Co. KG (Duisburg, Germany) in order to prepare it for use in the melt electrospinning system. The MM 4520 polyurethane exhibits a glass transition temperature of 45°C and a specific gravity of 1.25 according to material data provided by the supplier [173].

2.2 Equipment

The melt-electrospinning setup was custom built in-house for this study.

The system consists of five major parts, these being the heating and heating control system, the electrical field generation system, the spinneret positioning system, the material extrusion system, and the fiber collection system (Figure 1). These systems are described in more detail in the following sections.

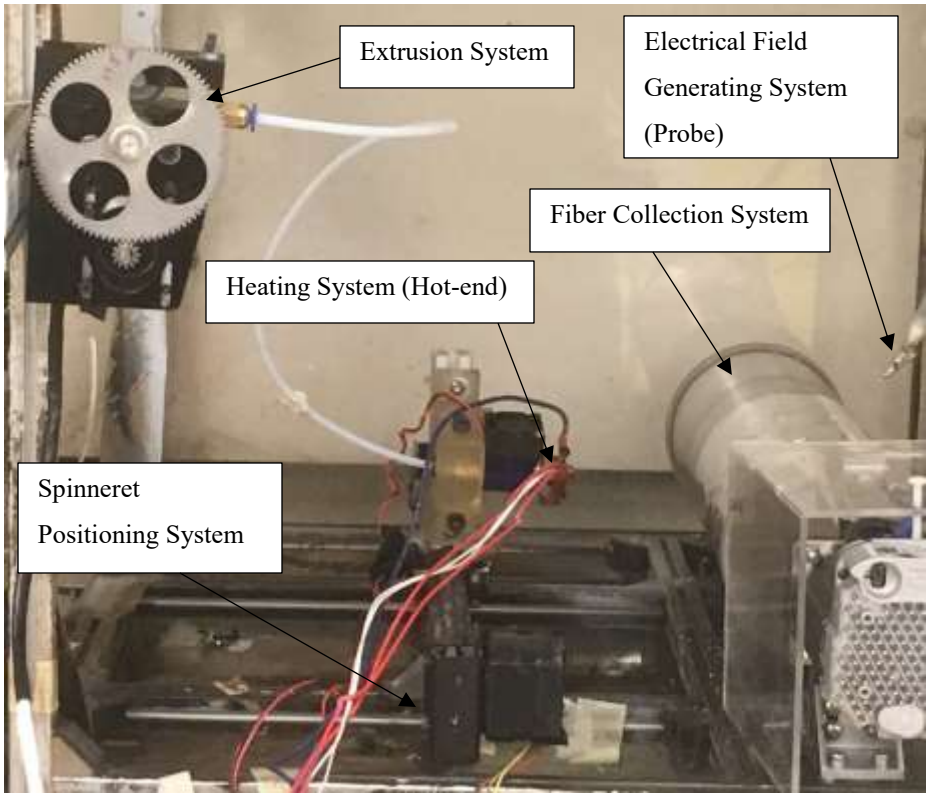

(A)

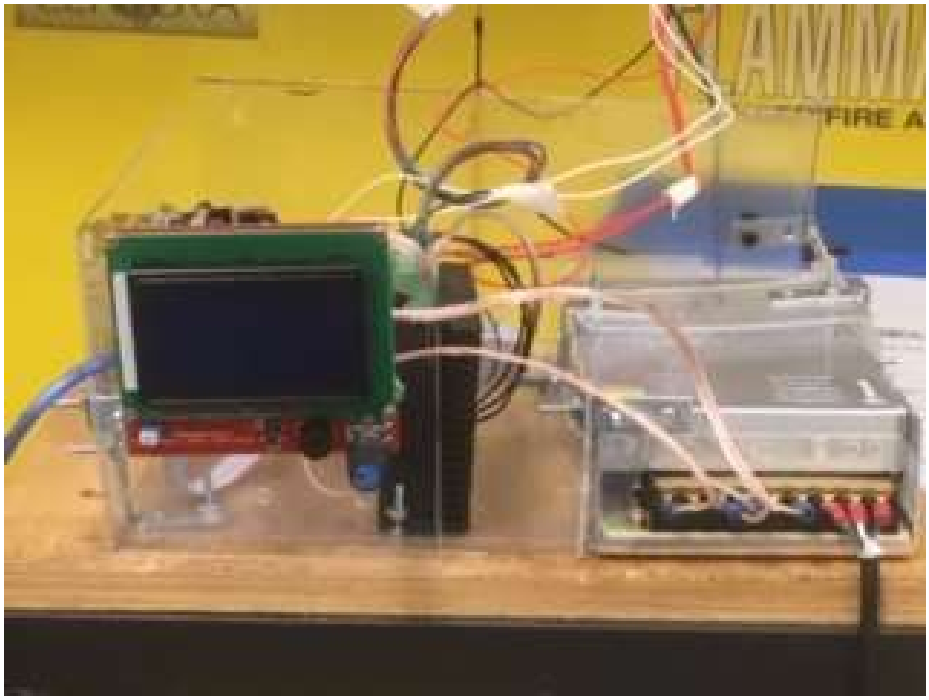

(B)

Figure 1. Melt-Electrospinning Setup A) Spinning Equipment B) Control Equipment

2.2.1 Heating and Heating Control System

The MM 4520 filament is heated into the necessary molten stage using a 3-D printing hot-end and the heating control system, presented in Figure 2.

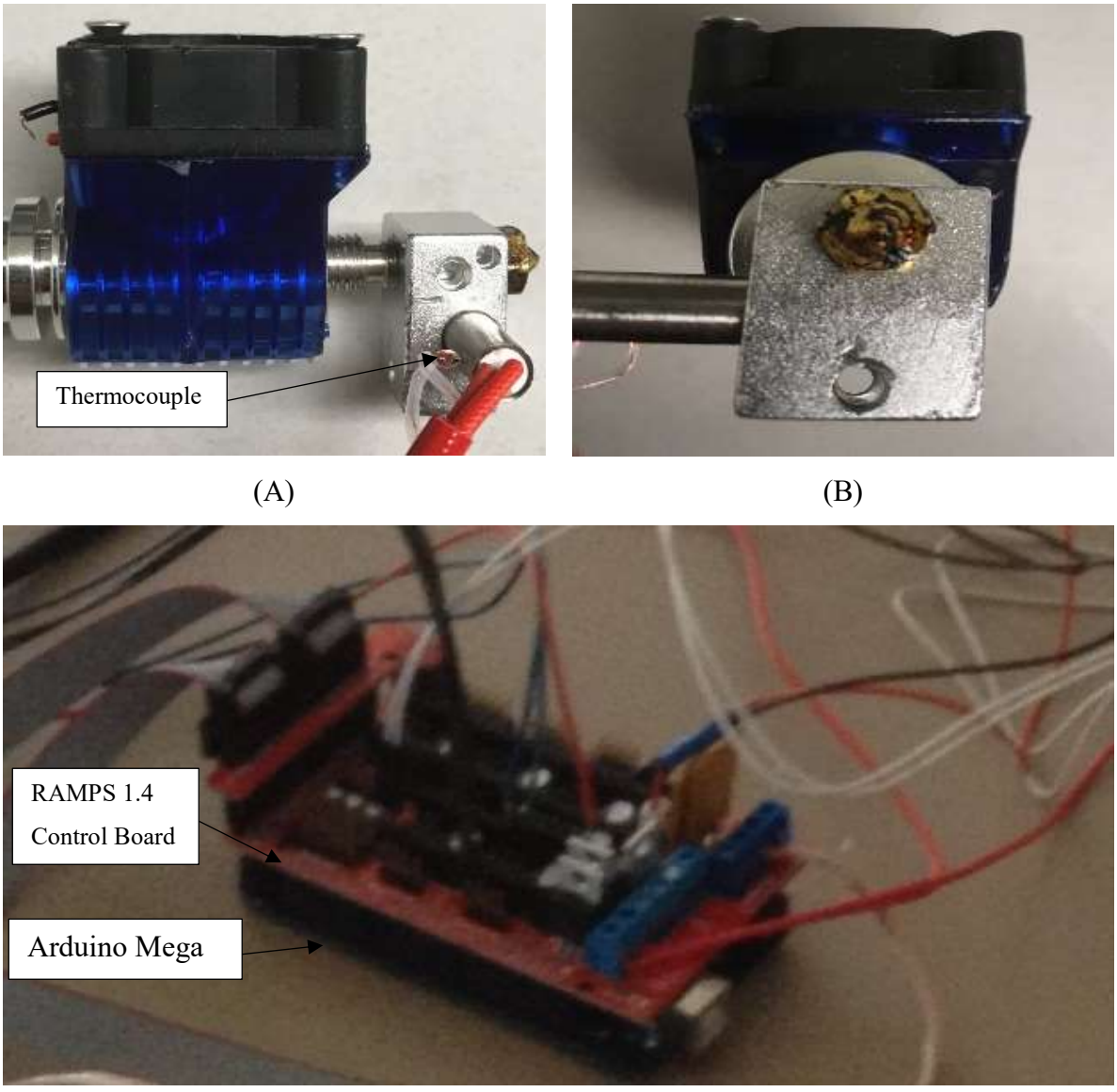

Figure 2. Heating and Heating Control System A) Hot-end Side View (Derived from 3-D printer hot-end) B)Hot-end Front View (Derived from 3-D printer hot-end) C) RAMPS 1.4 control board pared with Arduino Mega

In order to control the temperature of the hot-end, a RAMPS 1.4 control board/ Arduino Mega setup running open source Marlin firmware (Marlin 1.1.8) [174] modified for the specific

circumstances of this work was used. A thermocouple in the heating block of the hotend was hooked into the RAMPS 1.4 board to allow for full PID control of the system. A system using a similar open source 3-D printing hot-end setup in order to achieve successful melt-electrospinning has been previously presented by Rivera and Hudson [175].

2.2.2 Electrical Field Generation System

The electrical field used to initiate the melt-electrospinning process was generated using an ES-100 high voltage generator procured from Gamma High Voltage Research (Ormond Beach, Fl. ,USA). This source is able to produce a voltage potential up to 100 kV [176] . The voltage source is presented in Figure 3. In order to insulate the electronic systems used to achieve the molten polymer state from the generated high voltage field, the voltage source was attached to the rotating drum target rather than to the spinneret, as has been presented in previous literature [145], [153], [175].

Figure 3-ES-100 High Voltage Source

2.2.3 Spinneret Positioning System

The spinneret positioning system allows for placement of the spinneret in the desired position by adjusting the x-position (spinning distance) of the nozzle tip. A diagram of the positioning with respect to the system can be found in Figure 4.

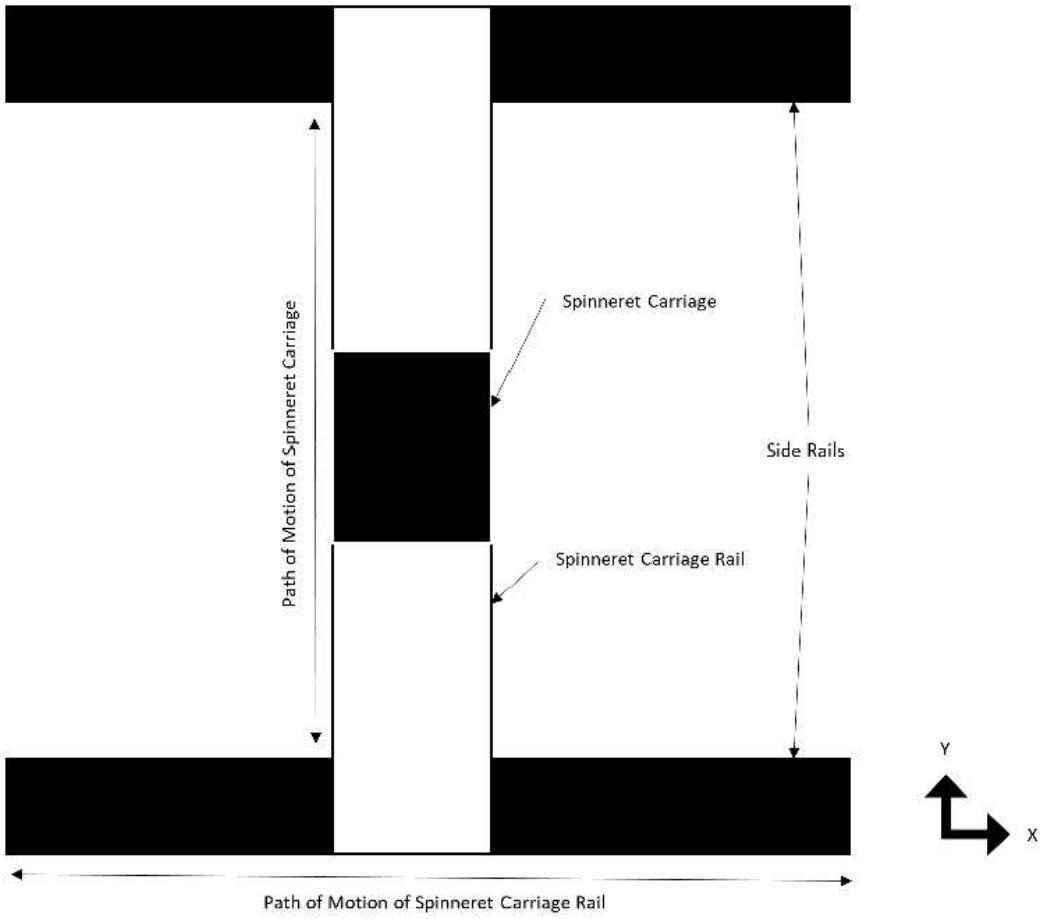

Figure 4- Spinneret Positioning System

The x position is controlled by moving carriage along the rails on which it is bolted as seen in Figure 4. In regards to the y axis positioning, due to the use of the translating carriage, the y axis position varies throughout the spinning process, controlled by the system. The z position (out of page), is fixed at all times throughout the melt electrospinning process.

2.2.4 Fiber Collection System

The fiber collection system consists of a charged rotating drum, an example of which can be seen in Figure 1. The rotational speed of the drum can be adjusted in order to control the randomness/alignment of the generated fibers. The drum is charged by attaching the high voltage source probe to a carbon brush attached to the outer surface of the drum. In order generate large randomly distributed non-woven mats of uniform thickness, while inducing an absolute minimum level of alignment, the rotational velocity of the drum is set to its minimal setting of 12 rpm.

2.2.5 Extrusion System

A 3-D printing gear based extruder purchased from ORD solutions Inc. (Cambridge, Ont., Canada) is used in order to move the polymer filament through the hot-end and into the high voltage field. The extruder can be seen presented in Figure 1. The gearing system seen on the extruder is used to control the movement of the filament.

As with the hot-end, the speed of the extrusion is controlled using the RAMPS 1.4 control board/Arduino Mega setup with Marlin firmware [174]. The extrusion speed is controlled in terms of mm/min of filament moved through the extruder, and thus through the hotend and into the high voltage field. In order to be able to lower the flow rate of polymer out of the system the stepper motor driver was set for $1/16^{th}$ micro-stepping, reducing the extrusion speed by a factor of approximately 8 from the speed input to the system.

2.3 Experimental Design

In order to examine the effect of varying melt-electrospinning parameters on the morphological, mechanical and shape memory properties of melt-electrospun shape memory polymer mats, the applied voltage and gap distance were both varied individually while all other parameters were held at constant levels, in order to allow any impact from the variation of these parameters on the properties of the final produced mats to be seen. Table 1 presents the constant parameters and the values at which they are set, and Table 2 presents the parameters which are varied in the present study, and the levels at which they are set.

Table 1- Constant Parameters during Melt-Electrospinning Process

Spinneret Diameter (mm)	Extrusion Rate (mm/min)	Spinning Temperature (°C)	Drum Rotational Velocity (RPM)	Spinneret Carriage Velocity (mm/s)
0.4	25	280	12	10

Table 2- Varied Parameters during Melt-Electrospinning Process

Level	Voltage (kV)	Gap Distance (cm)
+	20	10
-	15	5

With the parameters and levels described above, the final experimental design used in the preparation of the four fibrous mats, designated as T1-4 can be seen in Table 3.

Table 3- Experimental Design

	Generated Mat			
Varied Parameter	T1	T2	T3	T4
Voltage (kV)	15	20	15	20
Gap Distance (cm)	5	5	10	10

At an extrusion rate of 25 mm/min, not accounting for the diameter decrease at the nozzle, an approximate flow rate of 3.6 ml/hr of polymer is achieved assuming a constant filament diameter of 1.75 mm. It is noted that the flow rate that results from the extrusion setting on these tests is higher than what is reported in much of the literature [122], [145], [154], however it is in a similar order of magnitude to the extrusion rate seen in the work of Rivera and Hudson, who presented a similar melt-electrospinning device [175]. In the case of their work, their polymer was extruded at a rate of 10 mm/min [175]. As Rivera and Hudson also utilized a 0.4 mm nozzle as a spinneret in their work [175], along with similar 1.75 mm diameter filament [175], this indicates that the flowrates seen in the work presented here are not out of the range of expected values for a melt-electrospinning system utilizing a 3-D printing hot-end and extruder. This rate was chosen from a range of extrusion rates that was found to allow for continuous fiber generation with the current setup. It is believed that the reason for the necessity of the higher extrusion rate is due to the difference in the melt-electrospinning setup presented here. In systems where the molten polymer is held in a syringe, a relatively large volume of melt is available to be drawn by the electrostatic force, whereas in this extruder/hot-end system, only an extremely small amount of polymer is in a molten state at any one instant to be drawn into the gap.

In order to analyse the results of adjusting the various melt-electrospinning parameters on the mechanical, morphological and shape memory properties of the generated mats, the average values of fiber diameter, Young's modulus, yield strength, shape recovery ratio and shape recovery rate were found for each of the investigated parameter combinations.

2.4 Experimental Procedure

2.4.1 Mat Generation

2.4.1.1 Material Preparation

Prior to the beginning of sample generation, the MM 4520 filament was dried in a Lindburg Blue M™ vacuum oven (Thermo Scientific™ (Waltham, Ma, USA) -shown in Figure 5) for three days at 70°C.

Figure 5-LINDBERG BLUE M™ Vacuum Oven

The drying process was performed due to possible issues during the extrusion portion of the melt-electrospinning process due to moisture absorbed by the MM4520 [45]. Once dried, the filament

is vacuum sealed and stored in a desiccator and used within a week. Only dried filaments were used in the course of this work.

2.4.1.2 Equipment Preparation

Prior to the initiation of melt-electrospinning for each mat generation, the parameters were set according to the experimental design presented in Table 3, and the aluminium foil target was placed on the rotating drum as a substrate. Once the extrusion nozzle has reached the desired temperature the system was allowed equilibrate in order to ensure stable temperature throughout the spinning process.

2.4.1.3 Melt Electrospinning

Once the system was prepared, the drum was set to a rotational velocity of 12 rpm and the spinneret translation cart was set to a translational velocity of 10 mm/s. The high voltage source was then turned on and extrusion of the polymer was initiated. The system was allowed to run for 15 minutes, giving enough time for a mat to form. Following completion of the melt-spinning cycle, the mat was removed from the drum. All further testing was either completed within one week of initial sample generation, or the materials were dried at 70 °C in order to ensure moisture free samples.

2.4.2 Morphological Analysis

The morphology of the generated polymer-fiber mats, including the appearance of the fiber surfaces, fiber layout and fiber diameter was analyzed using scanning electron microscope (SEM) images of the generated mats. The SEM images were taken using a ZEISS EVO M10 Scanning Electron Microscope produced by ZEISS (Oberkochen, Germany).

One sample was taken from the top and bottom of each of the four mats generated in the course of this work. Figure 6 provides a visual representation of this sampling method.

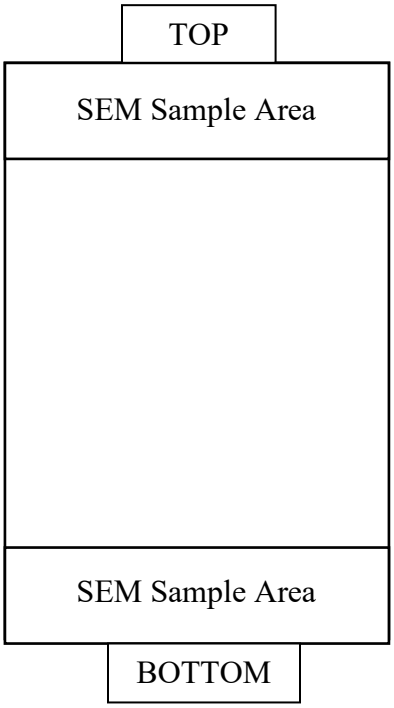

Figure 6- Diagram of SEM Sample Selection

A minimum of four images where taken in different sections of each of the samples, and four were selected from each set for analysis.

The SEM images are analyzed using Image J software [177] in order to determine an average diameter of the generated fibers, as well as other morphological features present in the mats. 10 fibers were selected in each image and 5 diameter measurements were taken along the length of each of the selected fibers. The average fiber diameter was determined by averaging the 400 fiber diameter measurements taken from each of the generated fibrous mats.

In addition to the images taken for fiber diameter characterization, close up images of the fiber surfaces were also taken in order to examine the effect of the spinning parameters on the surface morphology of the generated fibers.

2.4.3 Mechanical properties analysis

Mechanical analysis of the generated mats is performed using an Electroforce® 3200 produced by TA Instruments™ (New Castle, DE, USA). Samples of generated polymer fiber mats are made with theoretical dimensions of 10 mm by 35 mm, with a gage length of 15 mm. The gage length of 15 mm allowed for efficient use of the available extension range of the Electroforce®3200. The gage length of 15 mm was previously reported by Hacker et al. when testing melt-electrospun modified polyurethane mats [154]. The width of 10 mm has been reported being used in tensile testing samples of electrospun fiber mates in the literature [92], and was selected due to the ease of working with this sample size. The tests were carried out under a tensile load at a strain rate of 10 mm/ min (inputted as 0.167 mm/s), which has also been seen in working with electorpsun SMP in the work of Budun, Isgoren, Erdem and Yuksek, who performed tensile tests on solution electrospun fiber mats of a similar polymer sourced from SMP Technologies Inc. (Tokyo, Japan) [92], as well as the work of Hacker et al. with melt-electrospun modified polyurethane mats [154]. All tensile tests were run using a 10 N load cell. Figure 7 presents a representative sample prior to and following the conclusion of tensile testing.

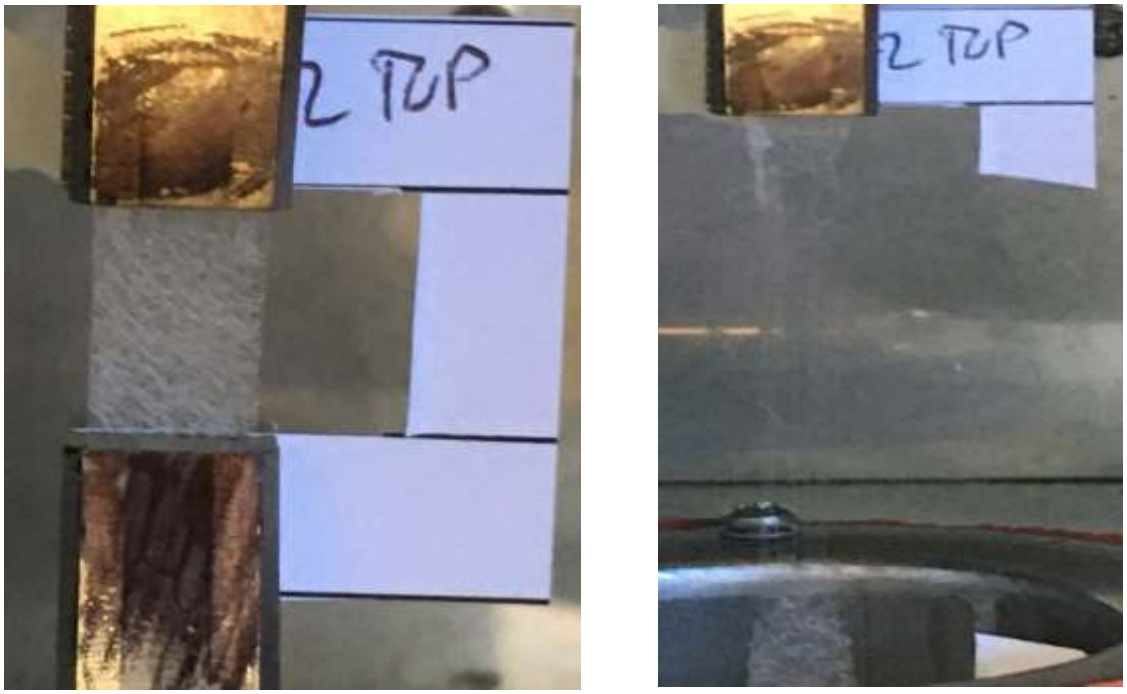

(A) (B)

Figure 7- Representative Mechanical Testing A) Prior to Test Initiation B) Following Test Completion

The load and extension data derived from the tensile tests is used to determine the Young's modulus and yield strength of the samples. Due to the extremely thin cross section of the melt-electrospun samples, the mats were folded over upon themselves twice in order to achieve a thicker specimen for testing purposes. As well, due to the thin cross section of the mats, it was not possible to utilize a cross section in the calculation of the stress present in the samples. In order to account for this, the method described below was used to determine the stress in the sample throughout the tensile test.

In order to determine the stress experienced throughout the course of the tensile test, the method presented by Ko and Wan in [178] is used, where the stress is determined by calculating the specific stress, which is in terms of the areal density of the mats, and then determining the stress by multiplying the specific stress by the density of the fibers which make up the mat [178]. For the use of this method, Ko and Wan defines the specific stress as in [178, Eq.(6.12)]

$$\sigma_{sp} = \frac{F}{w} * \frac{1}{\rho_A} \quad (1)$$

Where:

σ_{sp}: Specific Stress (N/tex)

F: Force (N)

w: Sample Width (mm)

ρ_A: Areal Density (g/m^2)

From this, the stress can be determined using [178, Eq.(6.9)]

$$\sigma = \sigma_{sp} * \rho_f \quad (2)$$

Where:

σ: stress (GPA)

σ_{sp}: Specific stress (N/tex)

ρ_f: Polymer density (g/cm^3)

The stress as defined in Equation (2) was then plotted against the strain developed in the sample during the course of the test. The strain at each point was defined as presented in Equation (3)

$$\varepsilon = \frac{L_d - L_g}{L_g} \quad (3)$$

Where:

ε: Instantaneous strain in Sample (mm/mm)

L_d: Instantaneous Displaced Length (mm)

L_g: Gage Length (mm)

2.4.3.1 Calculation of Young's Modulus

The Young's modulus of the samples was determined as the slope during the elastic range of the generated stress-strain curves. The Young's modulus was determined by the standard formulation presented in Equation (4)

$$E = \frac{\sigma_2 - \sigma_1}{\varepsilon_2 - \varepsilon_1} \quad (4)$$

Where:

E: Young's Modulus (MPa)

$\sigma_{1,2}$: Stress (MPa)

$\varepsilon_{1,2}$: Strain (mm/mm)

2.4.3.2 Calculation of Yield Strength

The yield strength of the samples was determined using the 0.2% strain offset method. The offset stress was determined using the offset strain and the Young's modulus of the sample as determined above. The yield strength was then determined as the point at which the offset line crossed the stress-strain curve.

2.4.4 Shape memory ratio / recovery rate analysis

The shape memory ratio and the recovery rate of the generated polymer-fiber mats are analyzed using a procedure consisting of two major steps, these being programming and recovery. In the programming phase, a sample of electrospun material with dimensions of 44 mm by 10 mm, and gage length of 24 mm was elongated using a Electroforce®3200 procured from TA

Instruments™ (New Castle, DE, USA) fitted with a thermal chamber to a strain of 25 % (6 mm extension) at a programming temperature of 50°C (T_g+5°C), at a rate of 0.01 mm/s.

The programming temperature was determined based on the work of Garces et al. which examined the shape memory properties of MM 4520 in cast form [45]. Following elongation, the system was allowed to cool to a temperature of at least 31.5°C (T_g -15°C±1.5 °C) in order to allow for the new shape to be fixed. Finally, the thermal chamber was opened so that the sample could be removed. Figure 8 presents representative images of the samples before and after the elongation process.

(A) (B)

Figure 8-Melt Electrospun Sample A) Before Programming B) After Programming

During the recovery step, the programmed sample was placed into a Lindburg Blue M™ vacuum oven with a weight attached to the lower end of the sample to maintain straightness throughout the test [45]. The weight used was measured at the beginning of recovery tests for each of the generated mats (T1-T4), and a tabulation of the average measured mass of the weight used

can be found in Table 4, and it is noted that the mass stayed essentially identical for each set of recovery tests performed over multiple days.

Table 4-Recovery Alignment Mass

	Generated Mat			
	T1	T2	T3	T4
Average Mass (g)	1.57	1.57	1.57	1.57
Standard Deviation of Mass (g)	5.61×10^{-4}	2.61×10^{-4}	2.39×10^{-4}	1.73×10^{-4}

The oven was heated to the recovery temperature of 70 °C as stated above, 25 °C above the Tg of MM 4520. The camera system was used to record images at a rate of 4 fps in order to record the sample as it recovers to its original un-deformed state. The images collected during this process are analyzed in order to determine the shape memory properties of the material, specifically the recovery ratio and recovery rate. Figure 9 presents representative images of samples before and after recovery.

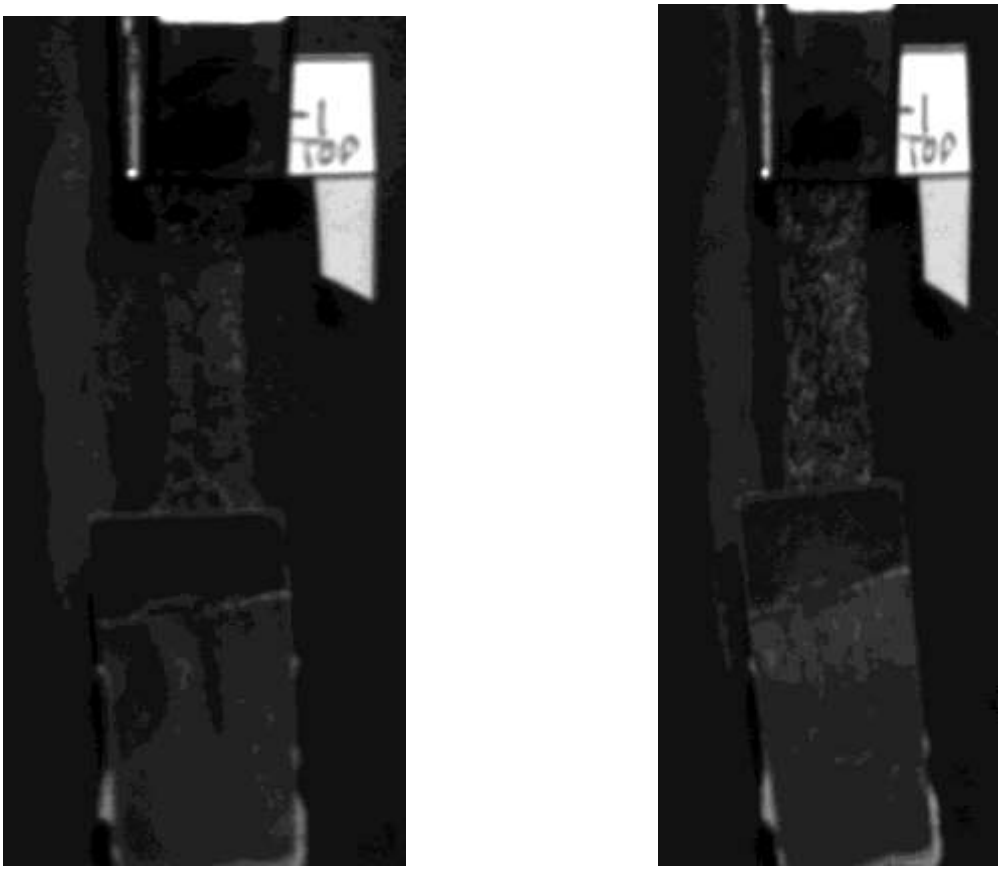

(A) (B)

Figure 9- Representative Shape Recovery A) At Beginning of Recovery B) Following Recovery Plateau

Following the collection of images, the length of the sample during the course of the recovery phase was measured at 50 frame intervals (12.5 s). These lengths were then used to determine the strain in the sample at each point, and these strains where then used to determine the recovery ratio (R_r).

The method used to calculate the recovery ratio of the melt-electrsopun mats was based on the work of Garces et al. , specifically in terms of the recovery ratio equation presented in [45, Eq.(6)] , as seen below:

$$R_r = \frac{\varepsilon_p - \varepsilon_r}{\varepsilon_p} \tag{5}$$

Where:

R_r: Recovery Ratio

ε_r: Strain remaining after recovery (mm/mm)

ε_p: Strain following sample programming (mm/mm)

Due to the possibility of error in the placement of the lower weight used to maintain straightness during the recovery process [45], ε_p in the denominator of Equation (5) was determined as the strain when the initially measured gage length underwent the prescribed 6 mm extension. The value of ε_p in the numerator of Equation (5) was determined as the strain based on the overall measured length of the programmed sample at the beginning of the recovery process.

The recovery rate was determined based on Equation (6) below:

$$V_R = \frac{L_p - L_r}{t_r} \tag{6}$$

Where:

V_R: Recovery Rate (mm/s)

L_p: Programmed Length (mm)

L_r: Post-Recovery Length (mm)

T_r: Time to Reach Maximum Recovery (s)

It is noted that the formulation of the recovery rate (V_R) presented in Equation (6) does not account for variation in the rate of recovery throughout the recovery process, and this analysis is used as a baseline to examine the speed of the recovery process, and does not necessarily represent the recovery rate at any one point during the process.

Chapter 3 Results and Discussion

3.1 Morphological Properties of Melt-Electrospun MM 4520

The fibrous mats generated through the melt-electrospinning processes are made up of individual constituent fibers. The morphology and diameter of these constituent fibers control the properties of the bulk mats, including the shape memory and mechanical properties. The variation of the two investigated melt-electrospinning parameters, namely spinning gap distance and applied voltage have their direct effect on the morphology and diameter of the fibers in the mats, and from there effect the other characteristics of interest. Therefore, the effect of varying the spinning parameters on the generated fiber morphologies and diameters are first discussed here, before moving to the other characteristics of the generated MM 4520 melt-electrospun mats.

3.1.1 Effect of Varying Melt-Electrospinning Parameters on Mat/Fiber Morphology

Figure 10 presents representative images of the melt-electrospun fibrous mats generated at each of the chosen parameter settings. In general with respect to the fibers making up these mats, it can be seen visually from Figure 10 that all parameter settings investigated in this work produced smooth fibers, with no beaded morphology seen to be present. Looking at the variation of the spinning parameters, it can be seen visually that the variation has an effect on the structure of the fiber layout. In Figure 10, it can be seen, qualitively, that increasing the applied voltage when the gap distance is held constant (Figure 10(A) vs (B) and Figure 10(C) vs (D)) appears to have a small effect on the structure of the mats in comparison to that of increasing the spinning gap distance when the applied voltage was held constant (Figure 10(A) vs (C) and Figure 10 (B) vs (D))

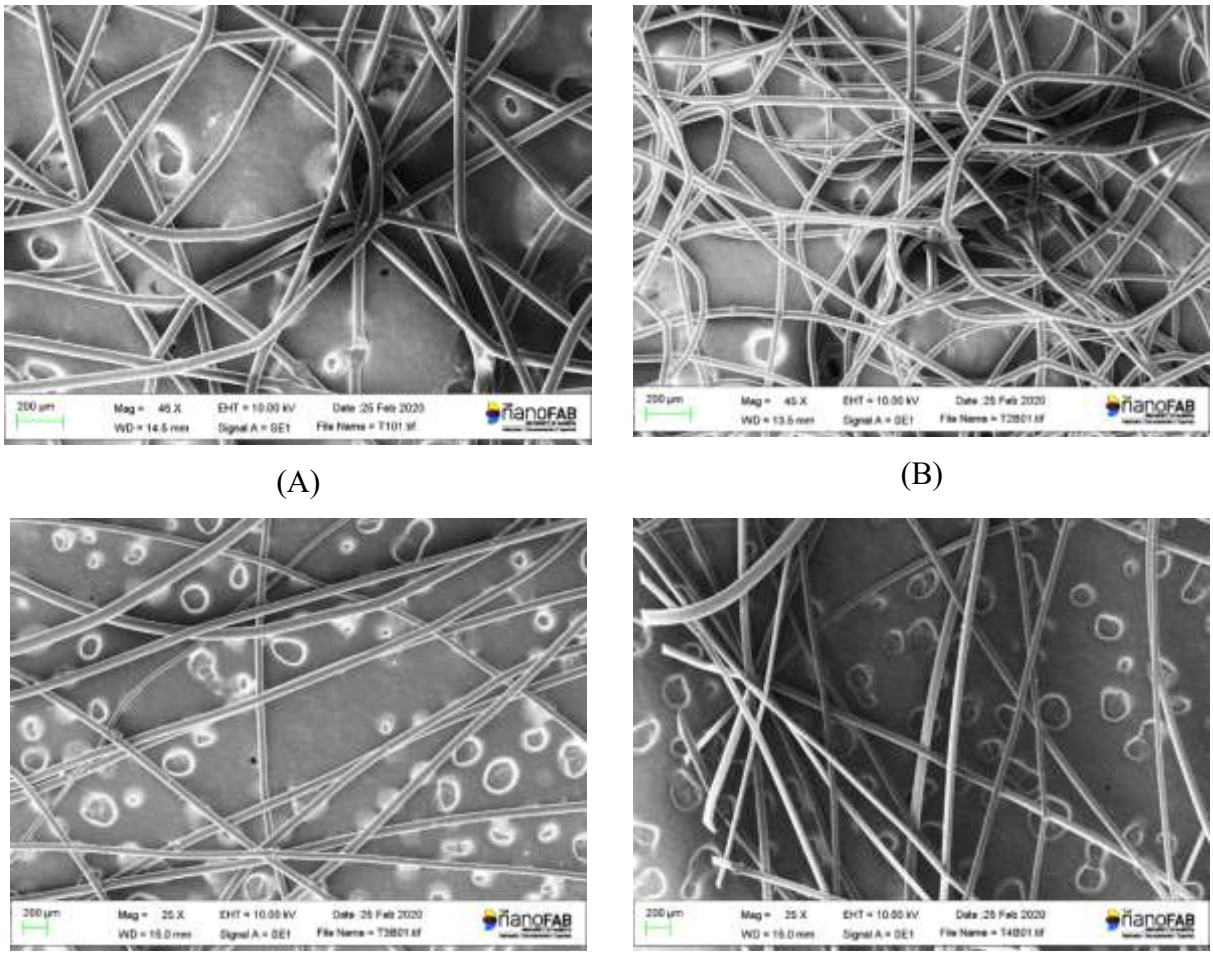

Figure 10- Fibers Generated at A) 5cm 15kV B) 5cm 20 kV, C) 10 cm 15 kV D) 10 cm 20 kV

In particular, in the constant spinning gap distance case, it can be seen that at 5 cm, as the voltage is increased(Figure 10(A) vs (B)), the randomness of the orientation of the fibers do increase, but both voltage levels still present a interwoven and partially coiled mat structure. In contrast, the mats generated at the 10 cm spinning gap distance (Figure 10 (C)-(D)) present very straight fibers, with little coiling or winding of the fibers present relative to those generated at 5 cm (Figure 10 (A)-(B)). When looked at in terms of the variation in the spinning gap distance a larger change in the structure is seen, with the variation at both 15 kV (Figure 10 (A) vs (C)) and 20 kV (Figure 10 (B) vs (D)) presenting shifts in structure from the more coiled and randomly curved fibers seen at 5 cm, to the straighter fibers seen at 10 cm. It is believed that this change is due to the larger change in the electrostatic force applied on the system when the gap distance was varied versus when the

applied voltage was varied. When the applied voltage was varied at constant gap distances of 5 cm and 10 cm, changes in the electrical field strength of 1 kV/cm and 0.5 kV/ cm where seen respectively. In contrast, when the spinning gap distance was increased from 5 cm to 10 cm at constant applied voltage levels of 15 kV and 20 kV, changes in the electrical field strength of 1.5 kV/cm and 2 kV/cm where found respectively. From these changes, it can be seen that larger magnitude changes in the electrical field strength occur when the spinning gap distance is increased versus when the applied voltage is varied, and this then results in the larger, more dramatic changes in the structure of the fiber mats when the spinning gap distance is varied at constant applied voltage levels.

In terms of the morphology of the fibers themselves, the variation of the spinning parameters chosen for this study do not appear to have any large effect on the surface of the generated fibers. Figure 11 presents representative close up images of the fibers generated at each of the parameter settings.

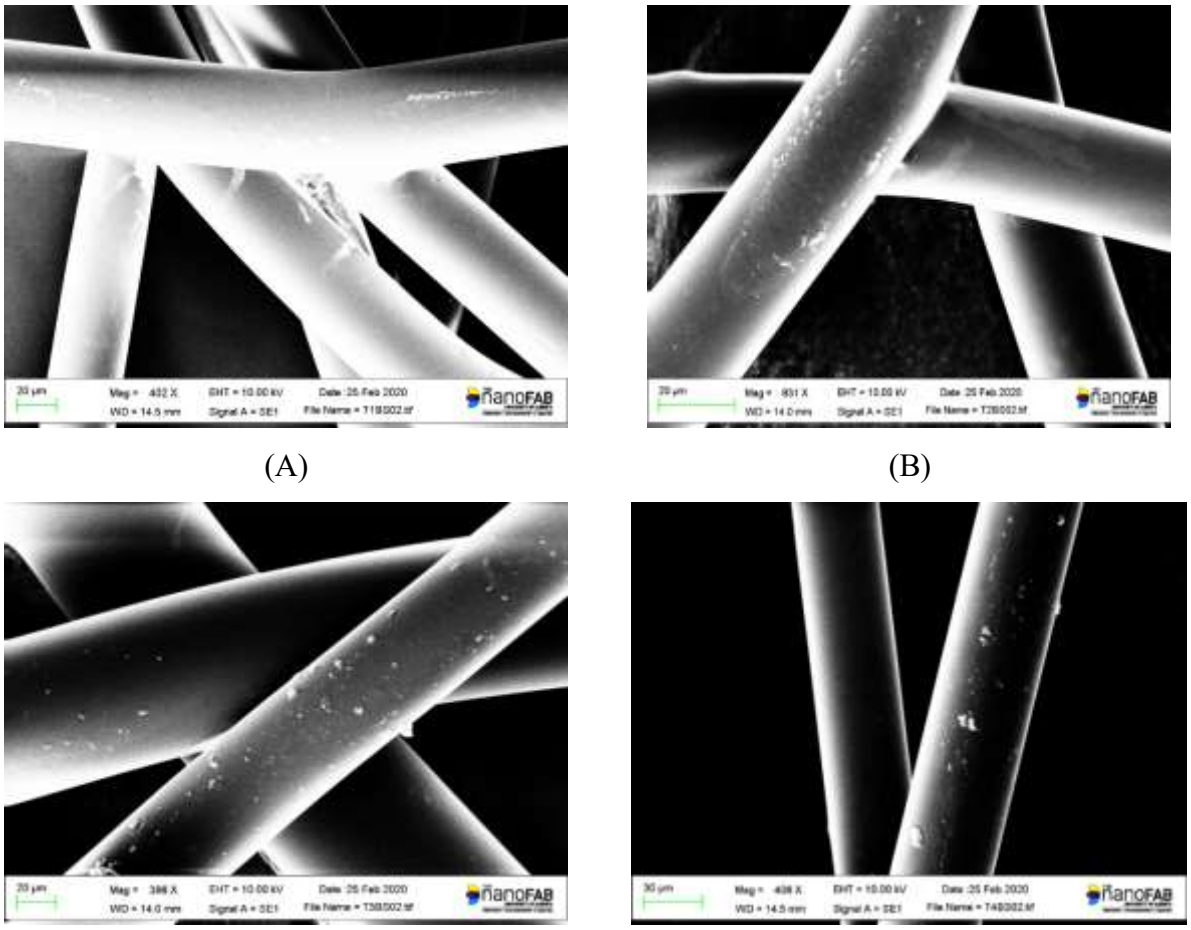

(A) (B)

(C) (D)

Figure 11- Close Up of Fibers Generated at A) 15 kV 5 cm Gap Distance B) 20 kV 5 cm Gap Distance C) 15 kV 10 cm Gap Distance D) 20 kV 10 cm Gap Distance

It can be seen from Figure 11 that at all spinning parameters solid cylindrical fibers were formed. While there does not appear outwardly to be any hard point connections between the generated fibers, it has been noted by Karchin et al. that it is difficult to state this with certainty based on SEM images [145], and that if these point bonds did not exist, the mats would have no integrity under any kind of external loading [145]. Therefore, while none is apparent on the SEM images, it is likely that point bonds do exist between at least some of the fibers. There do appear to be some imperfections on the surface of the fibers generated at the 5 cm spinning gap distance, as can be seen in Figure 11(A)-(B). These imperfections can likely be attributed to how the material cooled. The fibers generated at the 10 cm gap distance, which can be seen in Figure 11(C)-(D), appear to have some foreign debris on the fibers, and this is not believed to be related to the spinning process.

3.1.2 Effect of Varying Melt-Electrospinning Parameters on Fiber Diameter

3.1.2.1 Range of Generated Diameters

Through the variation of the spinning gap distance and the applied voltage, a range of fiber diameters were observed. Table 5 presents the average fiber diameters with respect to the parameters at which they were generated.

Table 5-Average Fiber Diameter's at Investigated Settings

	Applied Voltage (kV)	
	15	20
Spinning Gap Distance (cm)	Fiber Diameter (μm)	
5	48.0 ± 6.2	28.4 ± 6.8
10	73.6 ± 18.9	56.5 ± 16.0

As can be seen from Table 5, the generated fibers have average diameters ranging from a minimum of 28.4 ± 6.8 μm to a maximum of 73.6 ± 18.9 μm. The minimum value was produced with an electrical field strength of 4 kV/cm, while the maximum was produced with an electrical field strength of 1.5 kV/cm. The limited literature available on the melt-electrospinning of polyurethane [118], [125], [128], [145], [153], [154] presents a range of diameters from a minimum of 1.70 μm [128] to a maximum reported value of 40.35 μm [118]. While it is immediately noticeable that the lower end of the range of fiber diameters found in this study falls comfortably within the previously reported range, the upper end of the range, even when taken at the lower end of the range for the upper value of 73.6 ± 18.9 μm, this being 54.7 μm, falls outside of the range reported in the literature. The parameters utilized by Yan et al. in order to achieve the fiber diameter of 40.35 μm [118] appear to be similar to those used here to produce the fibers with average diameters of 73.6 ± 18.9 μm. Yan et al. utilized a applied voltage level of 15 kV, with a spinning gap distance of 10 cm [118], which is the same setting for these two parameters used in this work to achieve the largest fibers. They also utilized a melt temperature of 255 °C [118], which is lower than the 280

°C used in this work. In terms of nozzle diameter, it is not overtly clear in their work at which nozzle diameter the polyurethane fibers were generated. A likely cause for the larger fibers found at these vary similar parameters is described by Brown, Dalton, and Hutmatcher in their 2016 review of melt-electrospinning [152]. Brown, Dalton and Hutmatcher noted that when the spinneret was attached to ground and the collector is attached to the voltage source, less electrical charge density is available to draw the polymer across the spinning gap than if the same voltage was applied directly to the spinneret [152]. This charged collector, grounded spinneret setup is utilized in this work. With this in mind, the larger fiber diameters seen in this work compared to that reported in works such as Yan et al.'s where the spinneret is charged make sense in this case [118] . It should also be noted that while the majority of the values for average fiber diameter found in this study fall within the range seen in the previously published literature on the melt-electrospinning of polyurethane, all of these values lay on the upper end of the previously reported range. By looking at the electrical field strengths in previously published papers, we see a range from 0.57 kV/cm to 8.33 kV/cm [118], [125], [128], [145], [154]. Under this range we see that all but the largest diameter of 40.35 μm as reported by Yan et al. [118] are lower than all of the diameter found in this study. As discussed above, one reason for this is likely the phenomena related to grounding the spinneret discussed by Brown, Dalton and Hutmatcher [152]. Another possibility is related to the flow rate of polymer melt into the system. Of the previous works on melt-electrospinning of polyurethane, only Hacker et al. report a flow rate for their work, this being 0.1 ml/h [154]. Compared to this, the flow rate used in the present study is approximately 3.61 ml/hr. Hutmatcher and Dalton note that as flow rate increases or decrease, the same trend is seen in the fiber diameter [122]. Based on this, if the flow rate being used in this study is larger than then in the other works, as it is in the case of the work by Hacker et al. [154], then this is likely a contributing factor to the larger fiber diameters found in this work, along with the setup of the melt-electrospinning system.

3.1.2.2 Effect of the Variation of Applied Voltage on Fiber Diameter

The graphical representation of the change in the average fiber diameter of the generated specimens when the applied voltage was varied from 15 kV to 20 kV at constant spinning gap

distances of 5 cm and 10 cm can be found in Figure 12 and Figure 13 respectively. Table 6 presents the maximum and minimum possible changes in the average fiber diameter at the two constant gap distances due to the change in the applied voltage based on standard deviations.

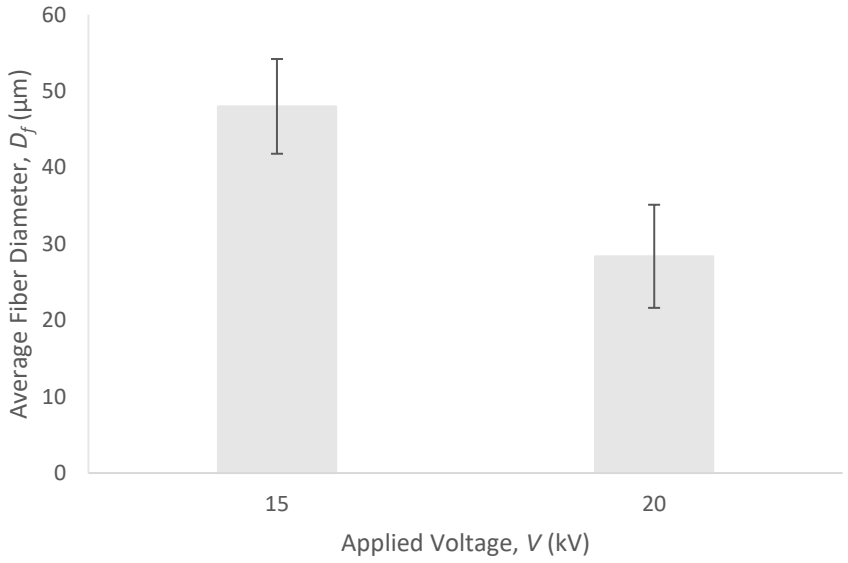

Figure 12- Change in Average Fiber Diameter with Varying Voltage at 5 cm Gap Distance

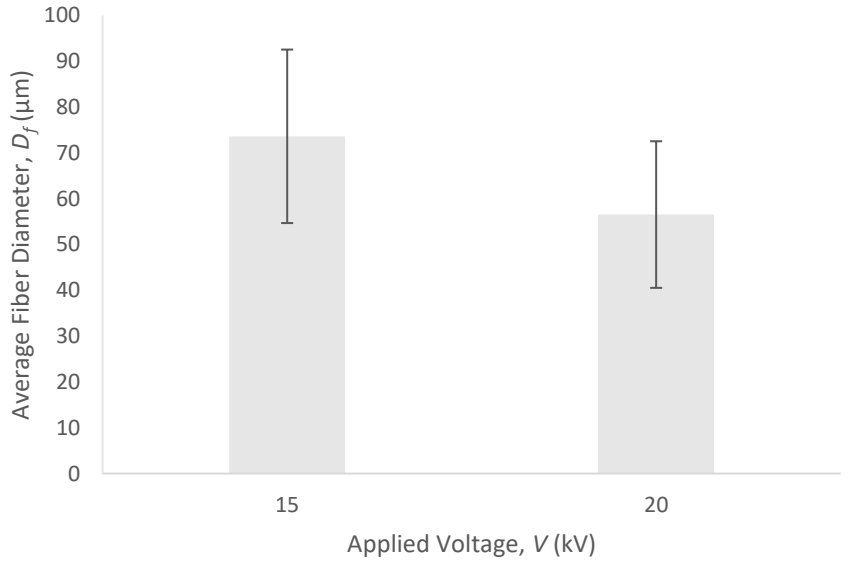

Figure 13- Change in Average Fiber Diameter with Varying Voltage at 10 cm Gap Distance

Table 6- Maximum and Minimum Change in Fiber Diameter at Constant Gap Distance and Varying Applied Voltage

Constant Gap Distance (cm)	Maximum Diameter Change (μm)	Minimum Diameter Change (μm)
5	32.6	6.68
10	52.0	-17.9

It is immediately apparent that while the change in voltage at a 5 cm spinning gap caused an apparent decrease in the average fiber diameter ranging from 32.6 μm to 6.68 μm, while no conclusion can be made when the gap distance was set to 10 cm due to the large standard deviations, as can be seen in Figure 13, making it possible that no variation occurs here.

The obvious cause of this discrepancy between the 5 cm gap distance and 10 cm gap distance is the variation in the change of electrical field strength due to the variation of voltage in the two cases. A higher electrical field strength in the melt-electrospinning system results in a higher electrostatic force on the polymer melt being extruded into the spinning gap, and this larger force results in the generated fibers being stretched more before hitting the target, resulting in smaller diameter fibers [125], [179]. At the 5 cm spinning gap distance, varying the voltage from 15 kV to 20 kV results in a change in the electrical field strength from 3 kV/cm to 4 kV/cm, a net increase of 1 kV/cm, whereas at the 10 cm gap distance, the electrical field strength increased from 1.5 kV/cm to 2kV/cm, a net increase of 0.5 kV/cm. Therefore, the change in the electrical field strength at the 5 cm spinning gap distance is twice the magnitude of the change that occurs at the 10 cm gap distance. As well, it is possible that the lower magnitude of the electrical field strengths at the 10 cm gap distance reduced the force acting on the polymeric jet to such a degree that even a larger change at this level would not impact the fiber diameter. These observations may account for the apparent larger decrease in fiber diameter at the 5 cm spinning distance when the voltage was increased from 15 kV to 20 kV, as a larger increase in the force applied to the polymer jet occurred at this setting. Of the literature found on the melt-electrospinning of polyurethane, only three works were found that investigate the change in the fiber diameter with respect to the applied voltage [125], [128], [153]. Of these papers, only the work of Dasdemier, Topalbekiroglu and Demir directly reported a similar trend to that seen in this work, namely the reduction of the

generated fiber diamter when the voltage level was increased [125]. While Li et al. report no direct trend when voltage is increased [128], at the edge cases of the range of voltage levels that they investigated, namely 8 kV and 24 kV, a change in the fiber diamter can be seen in their plotted results [128]. It should be noted that in the third study which investigated the effects of varying voltage on melt-electrospun polyurthane, namely the work of Mitchell and Sanders [153], they report an increase in the diameter of the generated fibers as they increased the voltage applied to the system [153]. Based on the graph they provide this appears as an initial decrease followed by an increase in the fiber diamter [153]. Mitchell and Sanders note that this response is different from what is presented in other reports, and seem to indicate that this is due to them using a gravity fed system rather than forcing their polymer at a consant rate into the field [153]. As the work performed for this study follows the more common method of forcing the polymer melt into the spinning gap at a constant rate, the apparent decrease in fiber diamter with increasing voltage strength at a constant spinning gap distance seen in this work when both the electrical field magntitue and change was high enough appears to agree with the other presentations of melt-electrospun polyuthane presented.

3.1.2.3 Effect of the Variation of Spinning Gap Distance on Fiber Diameter

Figure 14 and Figure 15 present the change in the fiber diameter when the applied voltage level was held constant at 15 kV and 20 kV respectively as the spinning gap distance was varied from 5 cm to 10 cm. Table 7 presents the maximum and minimum changes in the fiber diameter found at each of the constant voltage level when standard deviation of the measured values was taken into account.

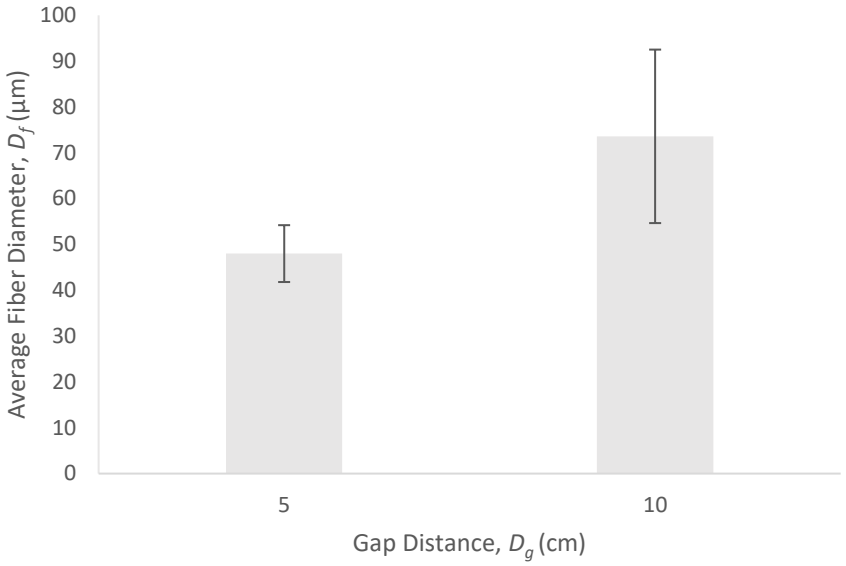

Figure 14- Change in Average Fiber Diameter with Varying Gap Distance at 15 kV

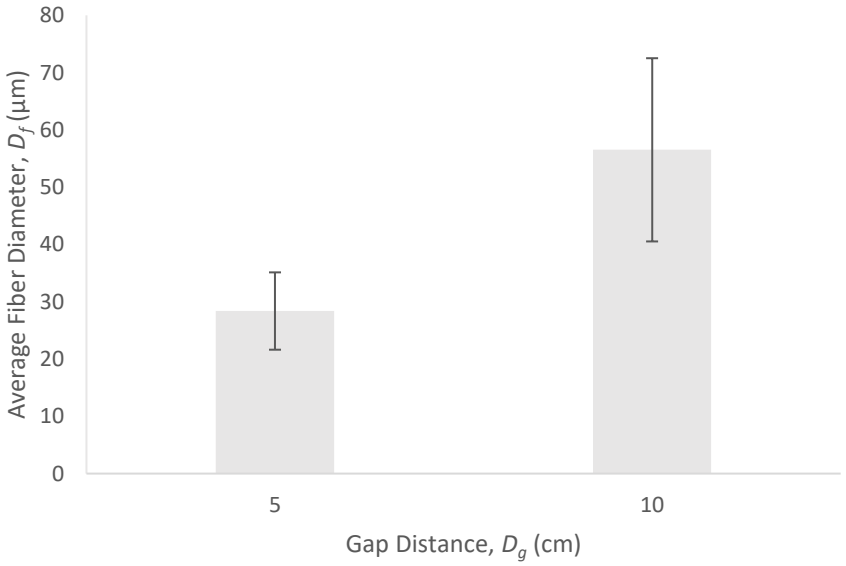

Figure *15*- Change in Average Fiber Diameter with Varying Gap Distance at 20 kV

Table 7-Maximum and Minimum Change in Fiber Diameter at Constant Voltage and Varying Gap Distance

Constant Voltage (kV)	Maximum Diameter Change (μm)	Minimum Diameter Change (μm)
15	50.7	0.455
20	50.9	5.40

In contrast to the effect which was seen with regards to varying the applied voltage at constant spinning gap distances, the change in gap distance at constant applied voltage levels resulted in apparent increases in the fiber diameter at constant voltages of both 15 kV and 20 kV as the gap distance was varied from 5 cm to 10 cm. In respect to the 15 kV constant applied voltage, the apparent change in fiber diameter from the 5 cm spinning gap distance to the 10 cm spinning gap distance ranged from a maximum of 50.7 μm to a minimum possible change of 0.455 μm when looking at the standard deviations of the average values. At 20 kV, this apparent change varied from a maximum of 50.9 μm to a minimum of 5.40 μm. As in the case when the voltage was varied at constant spinning gap distance, the main effect causing the fiber diameter to appear to increase as the spinning gap distance increased is believed to be the reduction in the electrical field strength as the spinning gap distance is increased [179]. Specifically, at the 15 kV setting, the electrical field strength decreases from 3 kV/cm to 1.5 kV/cm, while at the 20 kV setting, the electrical field strength decreases from 4 kV/cm to 2 kV/cm. Therefore, at 15 kV, the electrical field strength was reduced by 1.5 kV/cm, and at 20 kV, it was reduced by 2 kV/cm. It should be noted with respect to changing the spinning gap distance that the smaller resultant change in electrical field strength when the spinning gap distance was varied at 15 kV is greater than the larger change seen when varying the applied voltage at constant spinning gap distance. Therefore, for the parameter levels chosen for this study, changing the spinning gap distance causes a larger change in the strength of the electrical field, and therefore has caused apparent changes in the fiber diameter. As stated above, the literature on melt-electrospun polyurethane is limited. In the case of varying the spinning gap distance under constant applied voltage, only two of the studies found present any results [125], [153]. Dasdemir, Topalbekiroglu, and Demir present a change in the fiber diamter over their full scale of spinning gap distances of 6 cm to 10 cm at 40kV of 4.01 μm ±1.14 μm to 8.21 μm ± 2.34 μm [125]. The electrical field strength here changes from approximently 6.67 kV/cm to 4 kV/cm, a change of 2.67 kV/cm [125]. This presents a similar trend to that seen in the

work presented here, with the fiber diamter increasing as the electrical field strength decreases [125]. The work of Mitchell and Sanders consists of a vastly different setup then the standard melt-electrospinning setup, where their electrodes are independent of their collection surface [153]. Due to this it is harder to make a direct comparison to the work present in our study. It should be noted that while in the preseted work, a steady apparent increase was seen in the fiber diameter with increasing gap distance, this may not be representative of the actual trend due to the limited nature of the two level test employed. Zhang et al. note in their review of the subject that a trend of an intital decrease in the fiber diamter followed by an increase in fiber diamter has been reported by Qin et al. [179], [180]. While in the current work we see only the apparent increase in the fiber diamter, in the future it would be advantageous to expand the range and number of gap distances investigated in order to see if a more complex trend is present. Also a larger study with statistical analysis will be of great value.

3.2 Mechanical Properties of Melt-Electrospun MM 4520

The mechanical properties of the melt-electrospun MM 4520 fiber mats were determined based on the generated stress strain curves. Representative curves for each set of spinning parameters can be found in Figure 16.

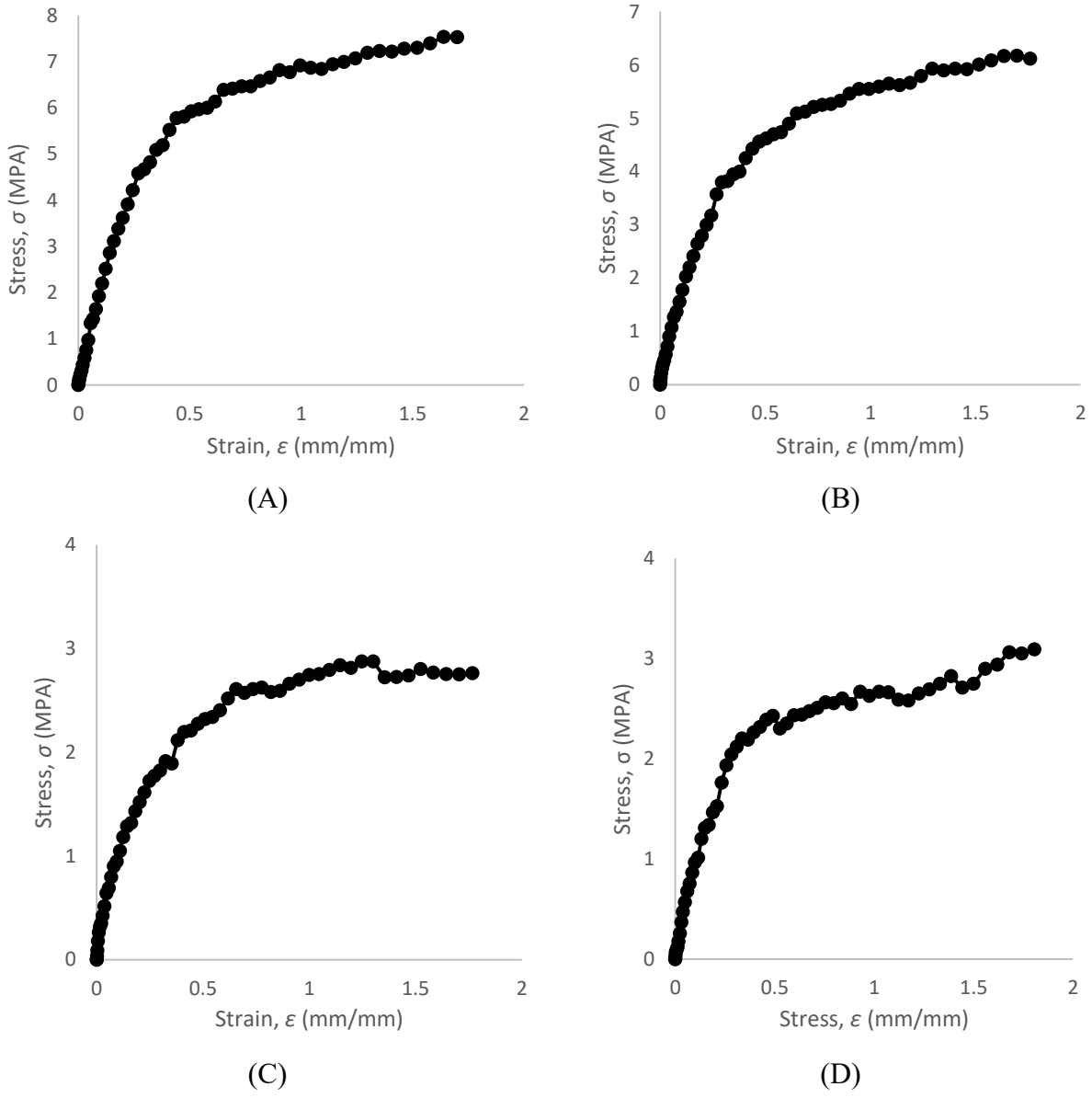

Figure 16- Representative Stress-Strain Curves for MM 4520 Fiber Mats Generated at A) 15 kV 5cm Gap Distance B) 20 kV 5 cm Gap Distance C) 15 kV 10 cm Gap Distance D) 20 kV 10 cm Gap Distance

Based on the curves presented in Figure 16, it can be seen that the generated mats all followed a generally standard stress strain curve of a ductile material.

3.2.1 Range of Young's Modulus values with Varying Melt-Electrospinning Parameters

Due to the variation of the spinning parameters, and through this the variation of the diameter of the generated fibers and morphology of the fibers and generated mats, a range of average Young's modulus values were found. These average values can be found in Table 8.

Table 8- Average Young's Modulus at Varying Spinning Parameters

	Applied Voltage (kV)	
	15	20
Spinning Gap Distance (cm)	Average Young's Modulus (MPA)	
5	14.2 ± 4.0	13.5 ± 2.50
10	8.38 ± 2.41	8.61 ± 3.85

From the data presented in Table 8, it can be seen that the average Young's modulus varies from 8.38 MPA ± 2.41 MPA at a spinning gap distance of 10 cm and applied voltage of 15 kV, to 14.2 MPA ± 4.0 MPA at a spinning gap distance of 10 cm and a applied voltage of 15 kV. Reports in the literature for the Young's modulus of melt-electrospun polyurethane are very limited. From these reports a range of values from 1.8 MPA ± 0.0 MPA [145] to 1.98 MPA ± 0.47 MPA [128] is seen. It is noted immediately that the values presented in the literature are lower than the values found in in this work with respect to the Young's modulus of melt-electrospun polyurethane. It has been noted in previous work on both melt-electrospinning and solution electrospinning that the mechanical properties of the generated mats are dependent on the morphology of the mats [145], [181]. In the previous report of the mechanical properties of melt electrospun polyurethane, Karchin et al. reported a very dense fiber mat [145], and the work of Li et al. also presents a mat which appears to be denser than those generated in this work [128]. As well Greenfeld, Sui and Wagner have noted that the Young's modulus of solution electrospun material increases with

decreasing fiber diameter due to higher alignment in the polymer chains caused by the larger forces necessary to reach the lower diameters [182]. They also note that this increase is seen after a critical diameter is reached, which is dependent on many of the solution spinning parameters [182]. This would likely account for the variation seen in the literature between solution electrospinning and melt electrospinning , where for example Li et al. reported a Young's modulus of 1.98 ± 0.47 MPa with fiber diameters varying from 1.70 μm – 2.53 μm in a melt electrospinning setup [128], while Budun et al., reported a much higher Young's modulus of 14.7 ± 3.2 MPA with a fiber diameter for the corresponding mat of 381± 165 nm [92]. It is noted here that in this work these kinds of changes in the fiber diameter are not seen, and it is thus not likely that the elongation is having a significant effect on the mechanical properties, though it may on other properties of the mats, which will be discussed later in this work. Other possible reasons for the variation in the results found in this work to that of other melt electrospun polyurethanes are as follows. Firstly, due to the mats being folded in order to conduct the tensile tests, it is possible that this tripling of the width of the mat, along with the folds present have resulted in an increase in the Young's modulus due to causing changes in the morphology. Due to the dependence on the morphology of the mats, it is difficult to directly compare the mechanical properties of the mats generated here to those found in the literature. While the reasons given above may account for the increased value, due to the fact that this method was used for all tensile tests completed in the course of this work, it is believed that the comparison between these mats made to examine the impact of the variation of melt-electrospinning parameters on the Young's modulus still give a valid understanding of the effect.

3.2.2 Range of Yield Strength Values with Varying Melt-Electrospinning Parameters

In the same manner as discussed for the Young's modulus, the measured yield strength varied between samples generated under varying spinning conditions. This data can be found in Table 9.

Table 9-Average Yield Strength at Varying Spinning Parameters

	Applied Voltage (kV)	
	15	20
Spinning Gap Distance (cm)	Average Yield Strength (MPA)	
5	4.27 ± 0.74	4.01 ± 0.67
10	2.13 ± 0.23	2.26 ± 0.72

The range of yield strength values were found to vary from 2.13 ± 0.23 MPA at a spinning gap distance of 10 cm and an applied voltage of 15 kV to 4.27 ± 0.74 MPA at a spinning gap distance of 5 cm and an applied voltage of 15 kV. The only previous report of the yield strength of melt-electrospun polyurethane that could be found was that of Li et al. [128]. They report a stretch yield stress of 0.9 ± 0.37 MPa [128]. It is noted that the yield strengths found in the work presented here are higher than those reported by Li et al. [128]. As well, it is believed that this slighter higher magnitude is likely due to similar morphological reasons as discussed in the case of the Young's modulus above.

3.2.1 Mechanical Properties Variation with Varying Melt-Electrospinning Parameters

3.2.1.1 Effect of Varied Voltage on Young's Modulus and Yield Strength

Figure 17 to Figure 20 present the change in the average Young's modulus and average yield strength at a constant spinning gap distance of 5 cm (Figure 17 and Figure 18) or 10 cm (Figure 19 and Figure 20) as the applied voltage is varied from 15 kV to 20 kV.

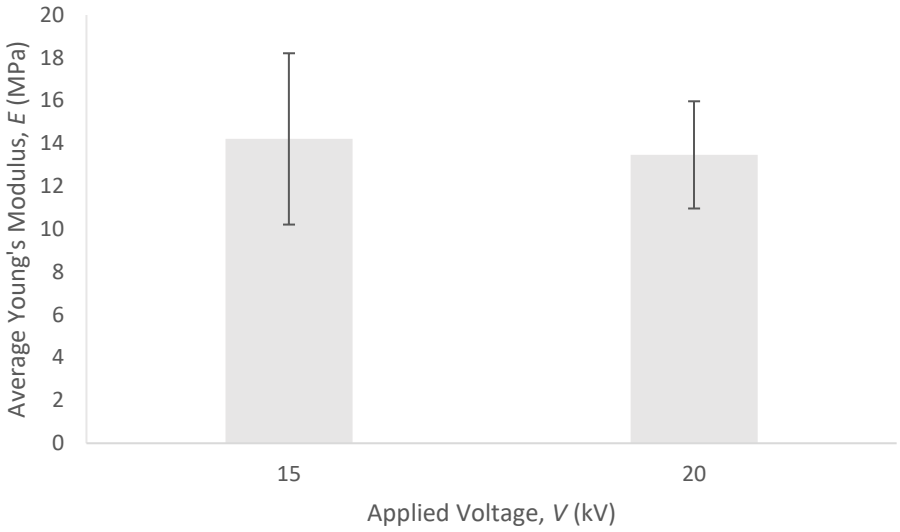

Figure 17-Change in Average Young's Modulus with Varied Voltage at 5 cm Gap Distance

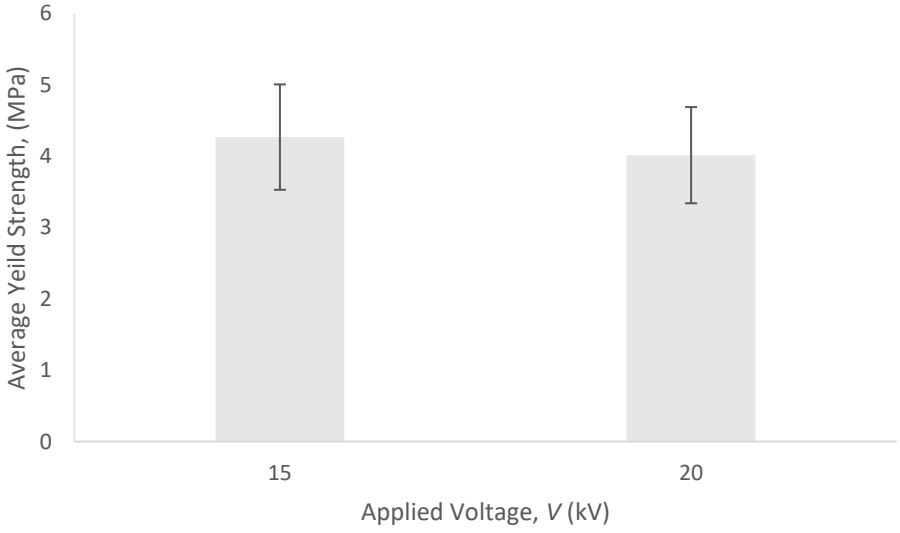

Figure 18-Change in Average Yield Strength with Varied Voltage at 5 cm Gap Distance

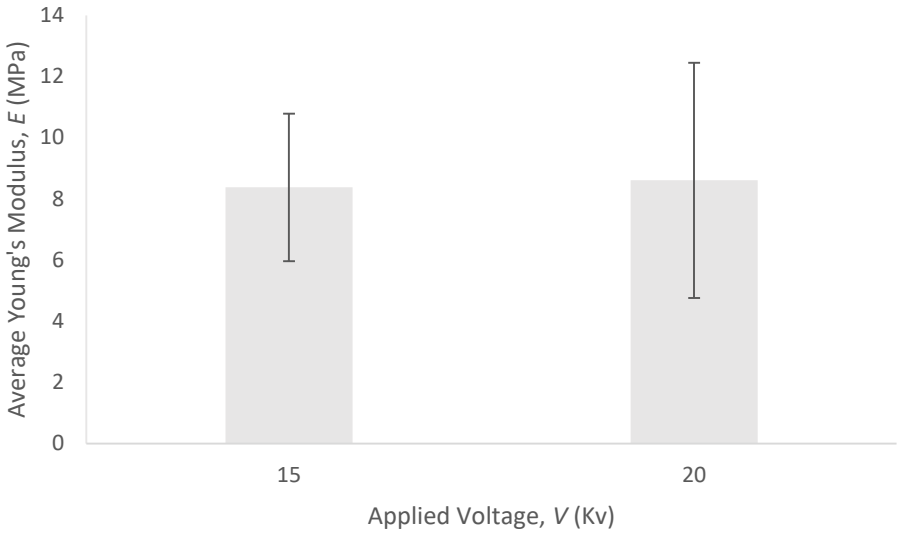

Figure 19-Change in Average Young's Modulus with Varied Voltage at 10 cm Gap Distance

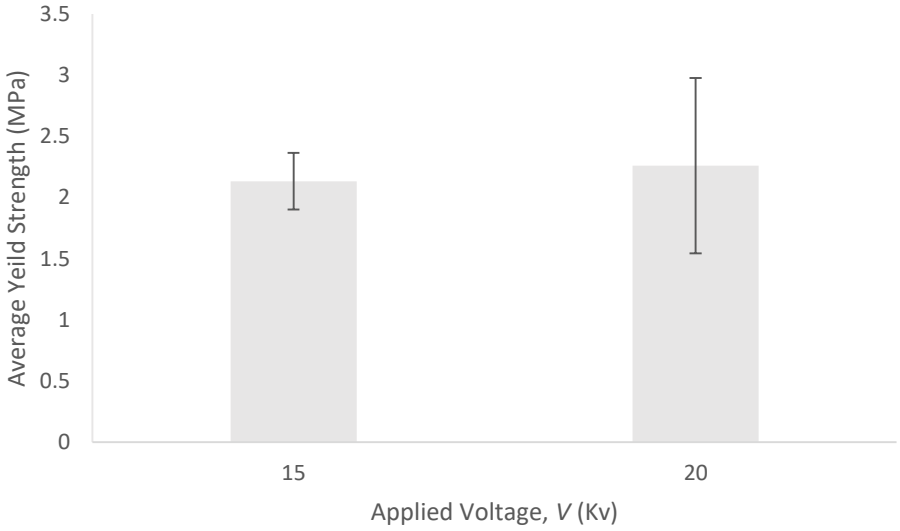

Figure 20- Change in Average Yield Strength with Varied Voltage at 10 cm Gap Distance

Table 10 present the maximum and minimum changes seen in the Young's modulus and yield strength as the applied voltage was varied over constant gap distance when the standard deviation was accounted for.

Table 10-Maximum and Minimum Change in Young's Modulus and Yield Strength at Constant Spinning Gap Distance

Constant Gap Distance (cm)	Maximum Change (Young's Modulus) (MPA)	Minimum Change (Young's Modulus) (MPA)	Maximum Change (Yield Strength) (MPA)	Minimum Change (Yield Strength) (MPA)
5	7.25	-5.76	1.67	-1.16
10	6.49	-6.03	1.08	-0.820

The minimum changes seen in Table 10, along with the data presented in Figure 17 through Figure 20 show that no conclusion can made respecting the effect of varying the applied voltage on the Young's modulus or yield strength, and no apparent change is seen in either due to the large standard deviations. Comparing this to the change seen in terms of fiber diameter over the same parameter ranges, it can be seen that when the voltage was varied at a 5 cm spinning gap distance, an apparent change was seen in the reduced diameter but not in the Young's modulus or yield strength, and that when the voltage was varied at 10 cm, no apparent change was seen in either the diameter or again in the Young's modulus or yield strength. Therefore it seems, in this case that at the 5 cm gap distance, the fiber diameter does not appear to effect the yield strength or Young's modulus.

3.2.1.2 Effect of Varied Spinning Gap Distance on Young's Modulus and Yield Strength

Figure 21 to Figure 24 present the change in the measured Young's modulus and yield strength as the spinning gap distance is varied at a constant applied voltage. Figure 21 and Figure 22 present the change in Young's modulus and yield strength respectively as the spinning gap distance was varied from 5 cm to 10 cm at a constant voltage of 15 kV, while Figure 23 and Figure 24 present the change in Young's modulus and yield strength respectively as the spinning gap distance is varied from 5 cm to 10 cm at a constant applied voltage of 20 kV.

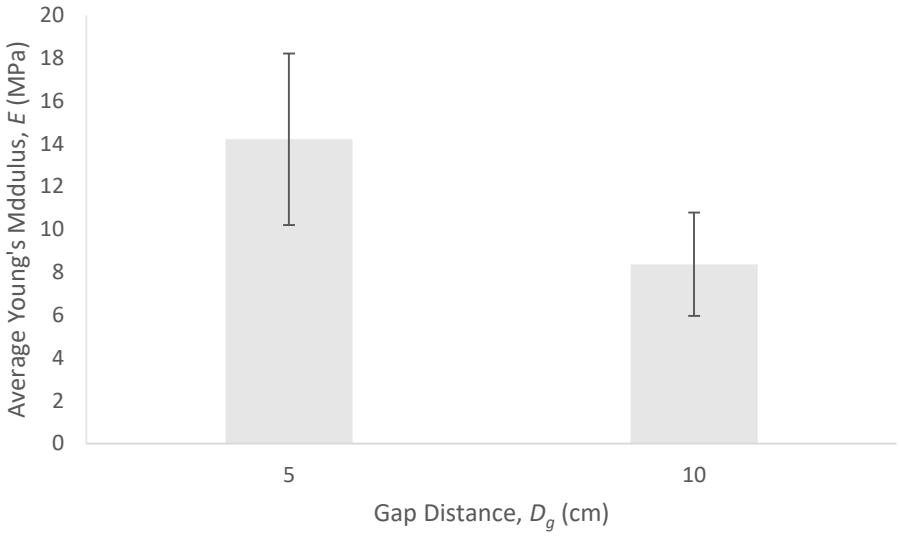

Figure 21- Change in Average Young's Modulus with Varied Gap Distance at 15 kV

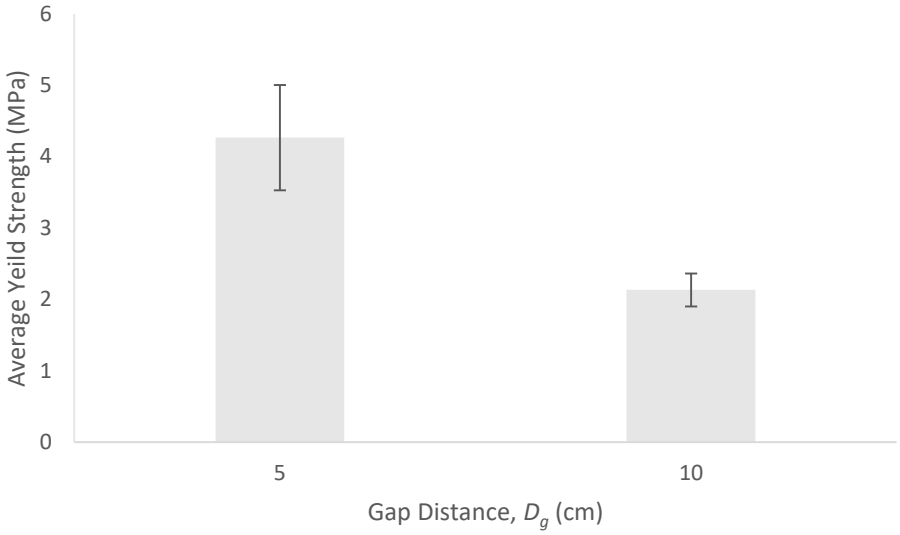

Figure 22- Change in Average Yield Strength with Varied Gap Distance at 15 kV

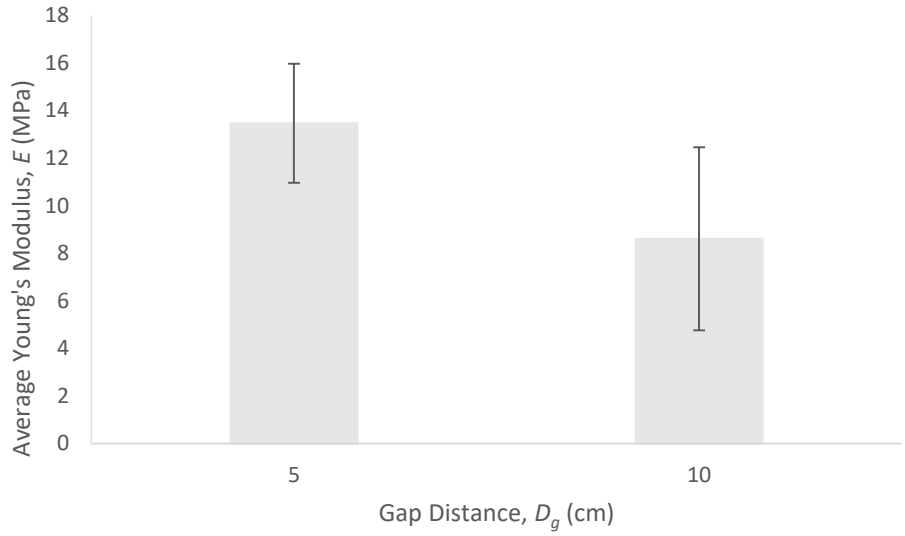

Figure 23- Change in Average Young's Modulus over Varied Gap Distance at 20 kV

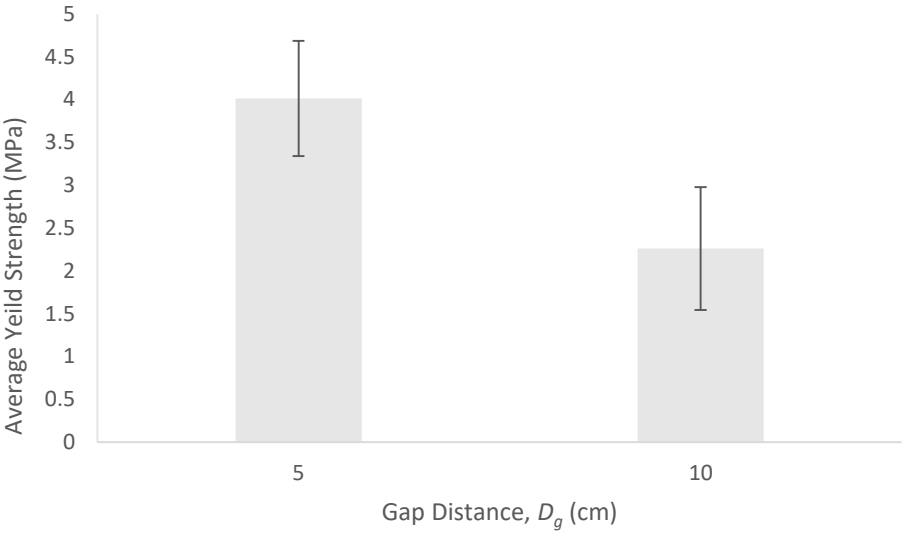

Figure 24- Change in Average Yield strength over Varied Gap Distance at 20 kV

Table 11 presents the maximum and minimum changes found for Young's modulus and yield strength at constant applied voltages when standard deviation is accounted for.

Table 11- Maximum and Minimum Change in Young's Modulus and Yield Strength at Constant applied Voltage

Constant Voltage (kV)	Maximum Change (Young's Modulus) (MPA)	Minimum Change (Young's Modulus) (MPA)	Maximum Change (Yield Strength) (MPA)	Minimum Change (Yield Strength) (MPA)
15	12.3	-0.575	3.10	1.17
20	11.2	-1.49	3.14	0.362

From Table 11 it can be seen that while no definitive conclusions can be drawn on effect on the Young's modulus with varying spinning gap distance due to the large standard deviations resulting in no apparent change being seen, there is an apparent change in the yield strength as the spinning gap distance was varied from 5 cm to 10 cm at both applied voltage levels, with minimum decreases in yield strength of 1.17 MPa and 0.362 MPa at 15 kV and 20 kV respectively rounded to three significant digits when accounting for standard deviation. In tying the changes directly back to the main spinning parameter that is being manipulated in these tests, that being the electrical field strength, the basic reasoning for the apparent larger changes when varying the gap distance at these levels at constant voltage over varying the voltage at constant gap distance is likely the larger change in electrical field strength seen when the gap distance is varied, which then will affect the morphology of the generated mats, and thus the mechanical properties presented here, and the reasoning for this effect will be discussed in the following section.

3.2.1.3 Effect of Fiber Diameter/Mat Morphology on Young's Modulus and Yield Strength

In general, the first observation to be made from the presented results is that no conclusion can be reached on the effect on the Young's modulus or the yield strength due to the change in fiber diameter over the presented ranges due to the large standard deviations. In terms of the Young's modulus, even in cases where the diameter has an apparent variation due to the variation of spinning parameters, no corresponding change in the Young's modulus could be seen. In terms of the yield strength, the data is not as clear cut, as for some variations in the fiber diameter, an apparent change in the yield strength was seen. However this was not seen in all cases where an apparent change in the fiber diameter occurred, as is the case when the voltage was varied from 15 kV to 20 kV at a 5 cm spinning gap distance. Due to this non-uniformity in effect, it is believed

that the change in diameter is not the direct cause for the change in the yield strength in cases where both changes occur. This apparent non-reliance on fiber diameter would thus seem to indicate that the critical diameter, and correspondingly the level of polymeric chain alignment needed to effect the Young's modulus and yield strength as presented by Greenfeld, Sui and Wagner is not being reached [182]. While, based on this data the diameter does not appear to be directly effecting these mechanical properties, other morphological properties may be having a significant effect.

When looking at the representative fiber morphology presented in Figure 10, a possible explanation for the effect that varying the spinning parameters on the mechanical properties on the generated mats can be seen, this being the orientation of the fibers in the produced mats. As presented in the previous section, when the voltage was varied at a constant spinning gap distance, no conclusion could be made on its effect on either the Young's modulus or the yield strength. In terms of the orientation of the fibers that make up the mats, while there may be a increase in the complexity of the orientation of the fibers, with an increase in coiling and winding when the voltage is varied from 15 kV to 20 kV at 5 cm, the large change in orientation occurs when the gap distance is varied at constant voltage as discussed previously. Comparing the trend in the Young's modulus and yield strength to the trend in the orientation of the fiber mats, a number of preliminary conclusions can be drawn. First, it appears based on the collected data, that the magnitude of the Young's modulus may not be tied to the orientation of the fibers mats. Specifically, it can be seen that while there is change in the fiber orientation of the mats, especially when the gap distance is varied, no change in the Young's modulus could be stated to occur. In contrast, when larger change in orientation is seen with the varying gap distance, a corresponding apparent change in the yield strength of the mat is seen, which may indicate a connection between the yield strength and the orientation of the fiber mat when a large enough change in the fiber orientation occurs. A possible explanation for this apparent connection between the yield strength and this change in the morphology of the generated mats is the rate at which individual fibers will come under direct loading during the course of the tensile tests. In a mat made up of more randomly distributed and orientated fibers, it would take a larger extension before a large portion of the fibers are carrying direct load, as they will need to be unraveled during the extension. In the case of a mat with straighter, less coiled fibers, as seen in both cases when spinning occurred at the 10 cm spinning gap distance, the individual fibers are more likely to be carrying the load from the beginning of

extension, and thus reach the constituent polymer's yield strength a lower level of extension than for the more chaotically orientated melt-electorspun mats. This morphological based understanding of what is occurring under the parameter variation presented here could also be seen to explain why the Young's modulus is not seen to have any apparent variations, while the yield strength does with the larger morphological change. In terms of the Young's modulus, there will always be some fibers under direct tensile load, either through the un-coiling of fibers or due to the straighter fibers, thus leading to the more consistent Young's modulus. In contrast, with respect to the yield strength, for the more coiled structure of the mats generated at the 5 cm spinning gap distance as one fiber begins to yield another will be coming under tension, maintaining the load bearing ability of the material and thus increasing the yield strength compared the straighter mat morphology seen in the samples generated at the 10 cm spinning gap distance, where final yield of the material would occur at a lower extension due to a smaller number of fibers becoming available to carry the load as the initially loaded fibers yield.

3.3 Shape Memory Properties of Melt-Electrospun MM 4520

Recovery tests were performed using the described procedures in order to determine both the recovery ratio and recovery rate of the generated mats. Representative recovery curves for mats generated at each of the four parameter combinations can be found in Figure 25 - Figure 28.

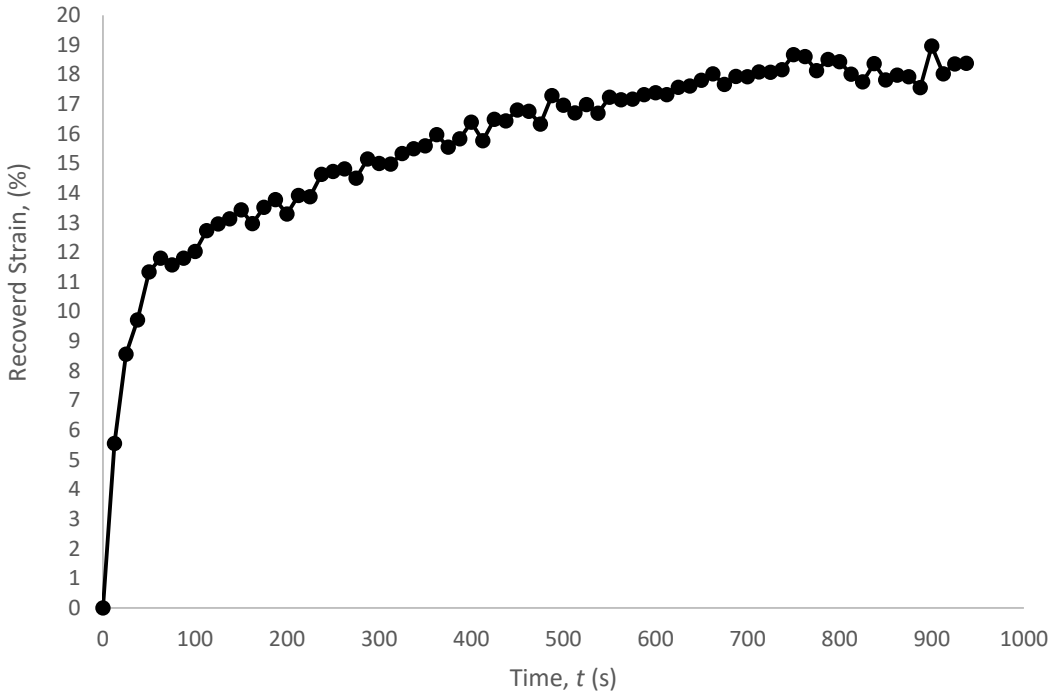

Figure 25- Representative Strain Recovery Curve for MM 4520 Fiber Mat Generated At 15 kV and 5 cm Gap Distance

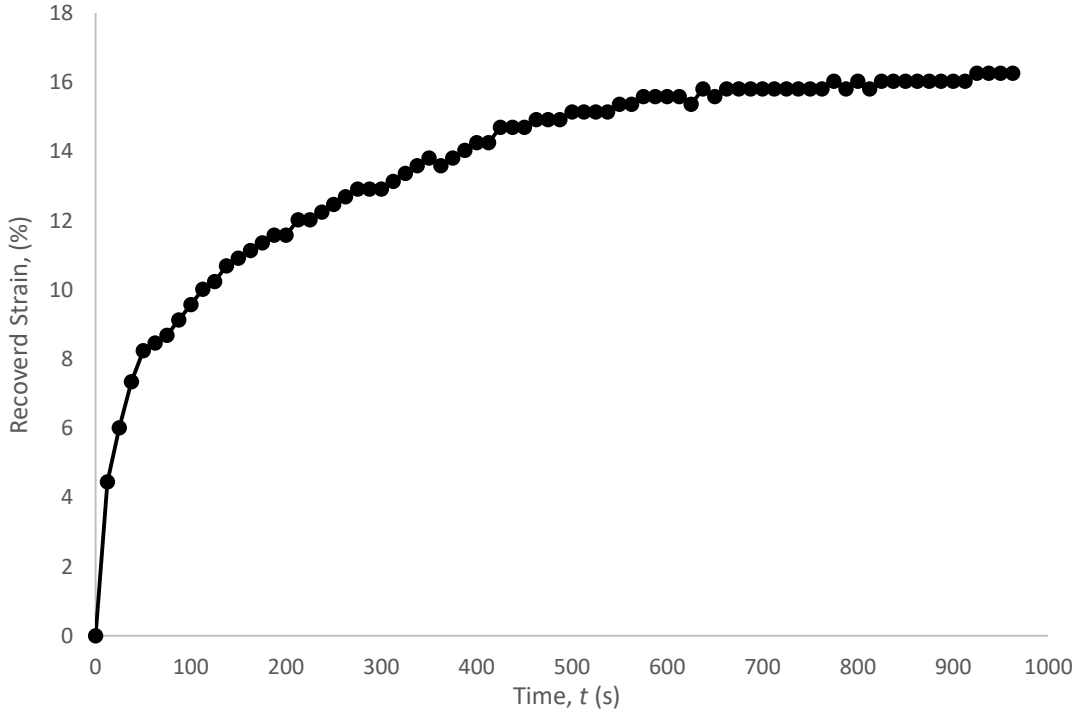

Figure 26- Representative Strain Recovery Curve for MM 4520 Fiber Mat Generated at 20 kV and 5 cm Gap Distance

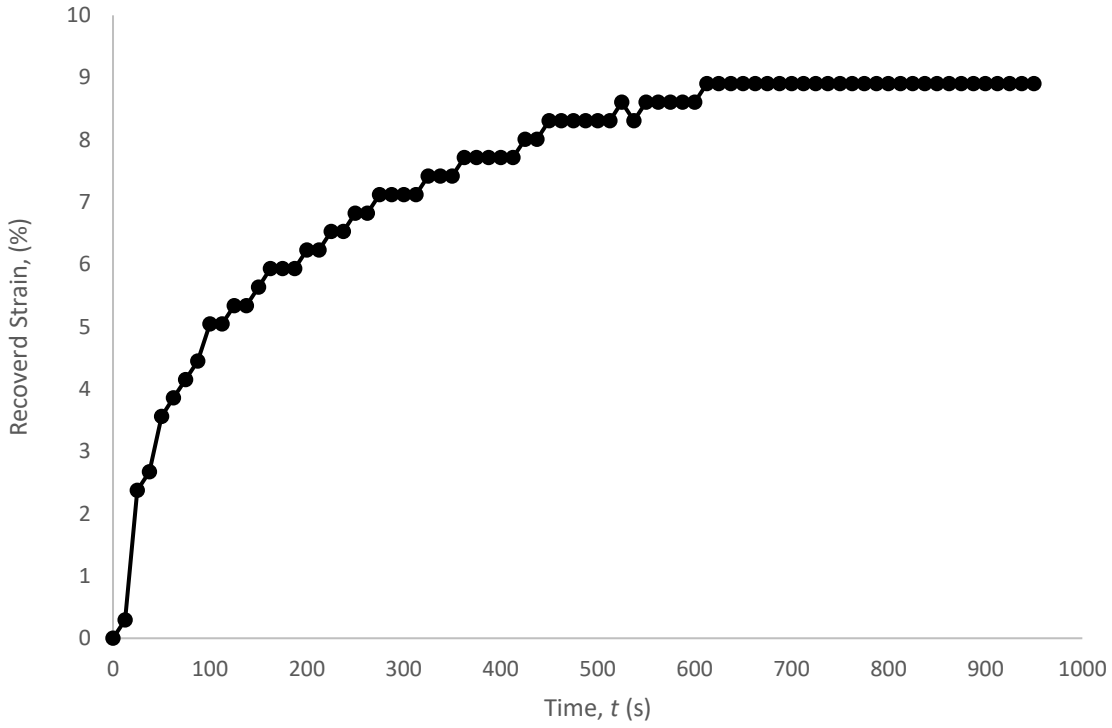

Figure 27- Representative Strain Recovery Curve for MM 4520 Fiber Mats Generated at 15 kV and 10 cm Gap Distance

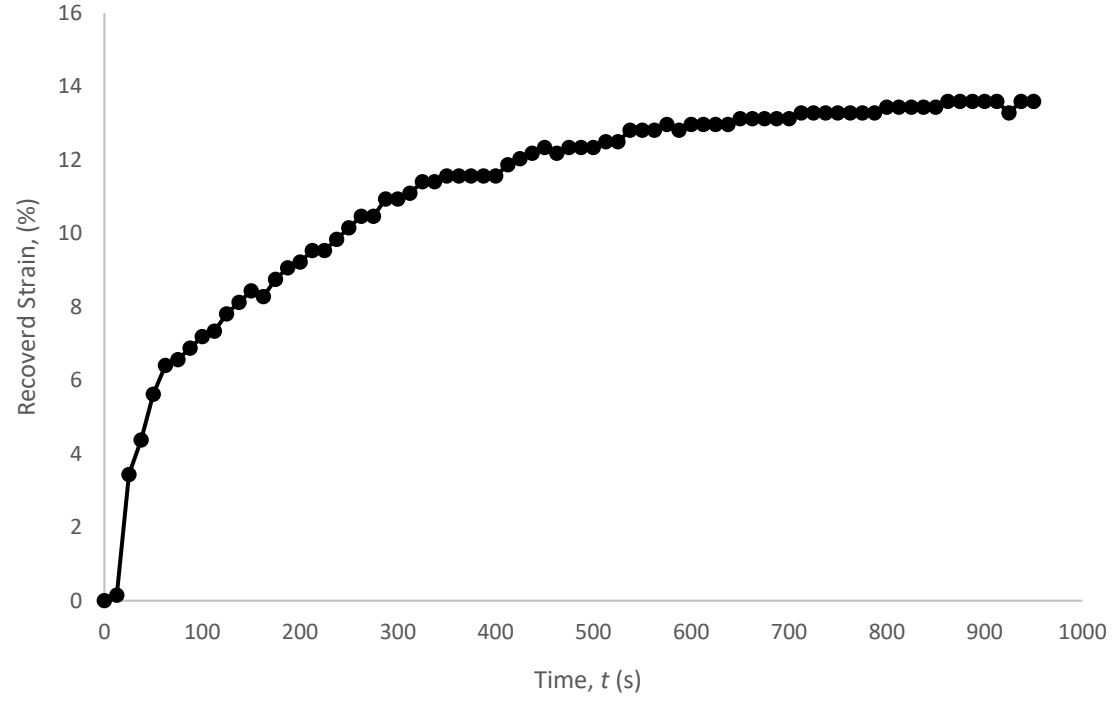

Figure 28- Representative Strain Recovery Curve for MM 4520 Fiber Mats Generated at 20 kV and 10 cm Gap Distance

The average results for the recovery ratio and the recovery rate found at each of the spinning parameters can be found in Table 12 and Table 13 respectively.

Table 12- Average Recovery Ratio at Investigated Parameter Settings

	Applied Voltage (kV)	
	15	20
Spinning Gap Distance (cm)	Average Recovery Ratio (%)	
5	61.9 ± 6.1	55.8 ± 5.2
10	33.2 ± 2.2	34.1 ± 13.0

Table 13- Average Recovery Rates at Investigated Parameter Settings

	Applied Voltage (kV)	
	15	20
Spinning Gap Distance (cm)	Average Recovery Rate (mm/s)	
5	0.00723 ± 0.00129	0.00550 ± 0.00051
10	0.00410 ± 0.00062	0.00475 ± 0.00072

From Table 12, it can be seen that the measured recovery ratio ranges from 33.2 ± 2.2 % when spun at 15 kV with a 10 cm spinning gap distance to a maximum of 61.9 ± 6.1 % when spun at 15 kV and a 5 cm spinning gap distance. While no previous work has been found on the melt-electrospinning of shape memory polymers, the literature on the recovery found for solution electrospun shape memory polymer polyurethane show a range from 70 % [95] to as high as 130 ± 4 % [92]. While it should be noted that comparing to the solution electrospun cases is not a one to one comparison with the melt-electrospun mats presented here, it can be used as a rough comparison. It is immediately noted that the maximum average recovery ratio seen in this work only reaches to the minimum value that was seen in the literature. With respect to the solution electrsopun polyurethane shape memory polymers, Budun et al. indicate that as the fiber diameters they achieved increased, the recovery ratio did the same [92]. On the other hand, work has been

presented showing that decreased fiber diameter in electrospinning situations results in more orientated polymer chains [99], [182], [183], and from this higher recovery ratios [99], and its impact on the presented work will be discussed in greater detail when the variation seen in the presented data is considered. This effect would seem to explain the difference between the lower recovery ratios found in this work and the higher ratios presented in the literature as discussed above, as the smallest diameter of the fibers found in this work were 28.4 ± 6.8 μm, while the largest fiber seen presented in the literature appear in the sub 3 micron range [92], [97], [98]. This represents almost a factor of ten difference between the fiber diameters presented here versus the those presented for solution spun materials, and would thus explain the difference from the values reported in the literature as described above. As well, it should be noted that as mentioned by Garces et al., the use of the small weight to keep the samples straight during the recovery process may have limited the extent of the recovery [45], which would also add to the reduction between the work presented here and the literature.

From Table 13, it can be seen that maximum average recovery rate found in this work was 0.00723 ± 0.00129 mm/s when the shape memory polymer mats were generated at an applied voltage of 15 kV and a spinning gap distance of 5 cm, while the minimum recovery rate was found to be 0.00410 ± 0.00062 mm/s when the mat was generated at an applied voltage of 15 kV and a spinning gap distance of 10 cm. A report by Leonés et al. working with PLA and PLA-OLA solution electrospun polymers presents recovery times, which when matched to their programming stretch of 5 mm appear to present total recovery rates in the same thousandths of a mm/s range [184]. In contrast, working with PCL-PDMS solution electrospun fibers, Kai et al. note that in one set of testing a sample stretched by 15 mm returned to its original shape after 3 s [93], which would correlate to a total recovery rate as defined in this work of approximately 0.12 mm/s [93]. While as seen, a range of possible recovery rates are present in the literature, those found in this work appear to fall within this range.

3.3.1 Shape Memory Properties Variation with Varying Mel-Electrospinning Parameters

3.3.1.1 Effect of Varied Applied Voltage on Shape Memory Properties

As with the previous properties of the electrospun mats, the effect of varying the applied voltage with gap distance held constant was investigated, and the change seen due to this variation in the applied voltage can be seen in Figure 29 and Figure 31 with regards to the recovery ratio, and Figure 30 and Figure 32 with regards to the recovery rate.

Table 14 presents the maximum and minimum change found for both the recovery ratio and the recovery rate when standard deviation was considered.

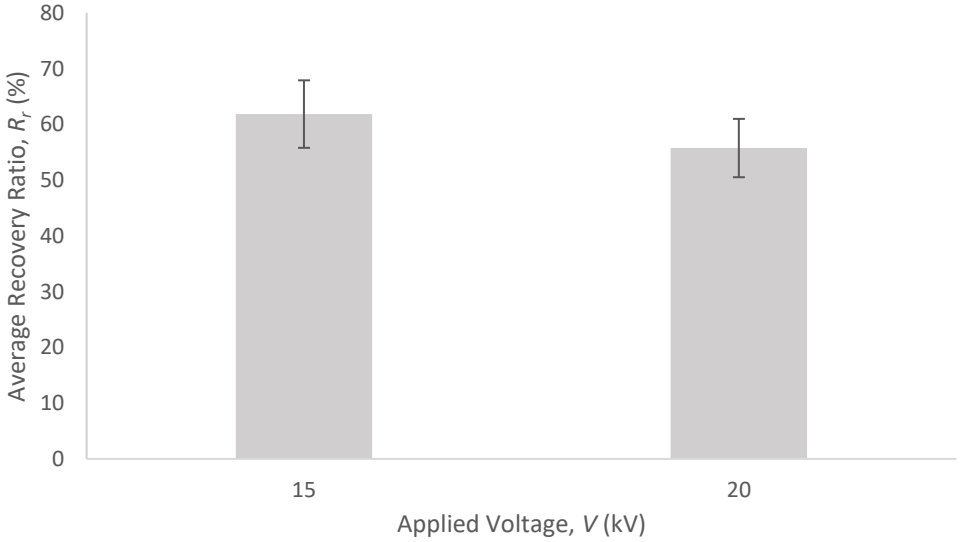

Figure 29- Change in Average Recovery Ratio over Varied Voltage at 5 cm Gap Distance

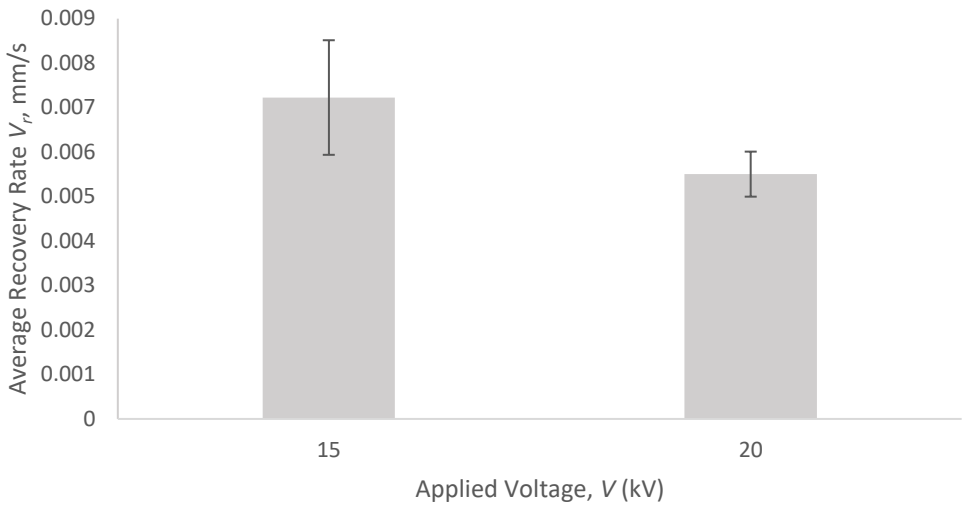

Figure 30- Change in Average Recovery Rate over Varied Voltage at 5 cm Gap Distance

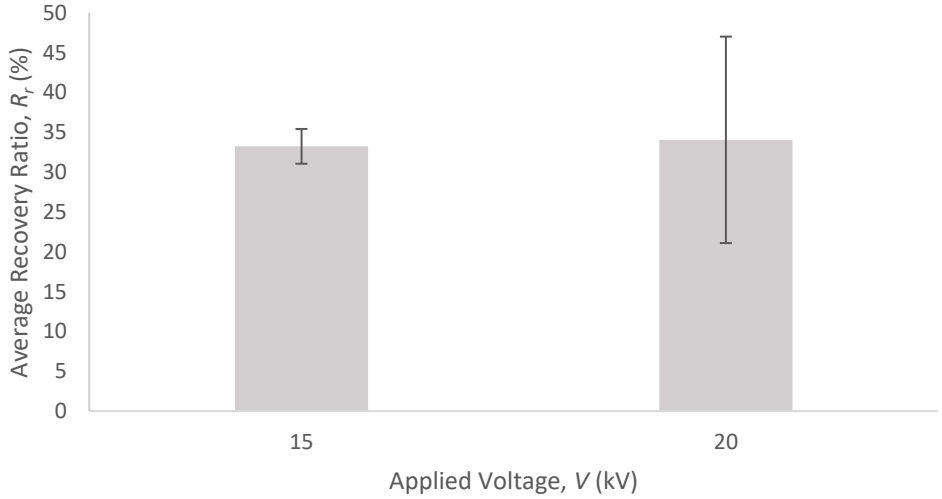

Figure 31- Change in Average Recovery Ratio over Varied Voltage at 10 cm Gap Distance

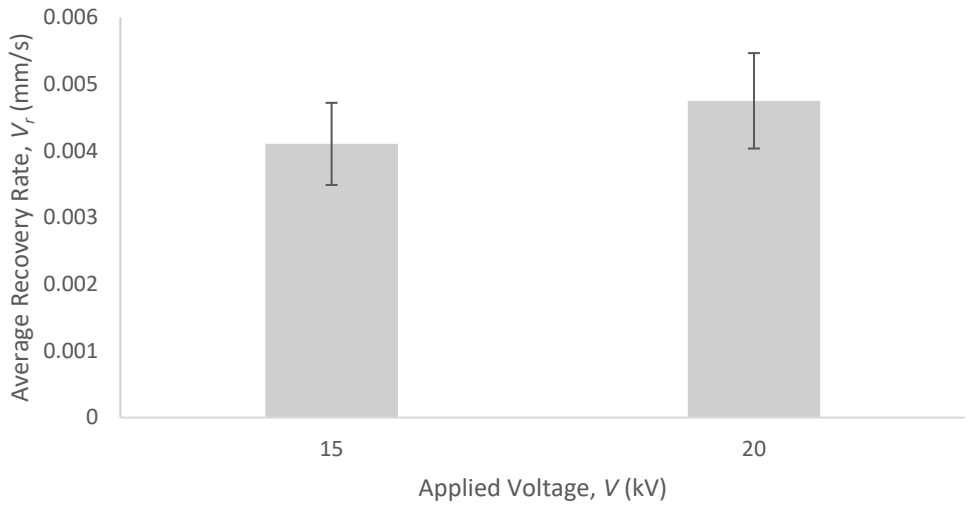

Figure 32- Change in Average Recovery Rate over Varied Voltage at 10 cm Gap Distance

Table 14- Maximum and Minimum Recovery Ratio and Recovery Rate at constant Gap Distance and Variable Applied voltage

Constant Gap Distance (cm)	Maximum Recovery Ratio Change (%)	Minimum Recovery Ratio Change (%)	Maximum Recovery Rate Change (mm/s)	Minimum Recovery Rate Change (mm/s)
5	17.4	-5.20	0.00352	-0.0000721
10	16.0	-14.3	0.00198	-0.000685

From Figure 29 - Figure 32, along with the maximum and minimum values found in Table 14, it can be seen that when applied voltage is varied over a constant gap distance at the parameter levels chosen for this work, no conclusions could be drawn with respect to change is seen in either the recovery ratio or the total recovery rate at either a spinning gap distance of 5 cm or 10 cm due to the overlap of the large standard deviations resulting in no apparent change occurring. This is comparable to the situation seen with respect to the mechanical properties due to the same variation. As discussed previously, the direct cause linked to the melt-electrospinning system of this lack of apparent effect could be due to the relatively small changes seen in the magnitude of the electrical field strength as the applied voltage is varied from 15 kV to 20 kV, and thus a smaller relative change in the electrical force which is acting on the polymeric jet.

3.3.1.2 Effect of Varied Spinning Gap Distance on Shape Memory Properties

In contrast to the effect of varying the applied voltage at constant gap distance as discussed previously, an apparent effect is seen when varying the spinning gap distance at constant voltage. These effects can be seen visually in Figure 33 and Figure 35 with regards to the recovery ratio at 15 kV and 20 kV respectively, and Figure 34 and Figure 36 with regards to the total recovery rate at 15 kV and 20 kV respectively. Table 15 present the maximum and minimum changes seen in the recovery ratio and total recovery rate due to the variation in the gap distance at both 15 kV and 20 kV applied voltage levels when the standard deviation was taken into account.

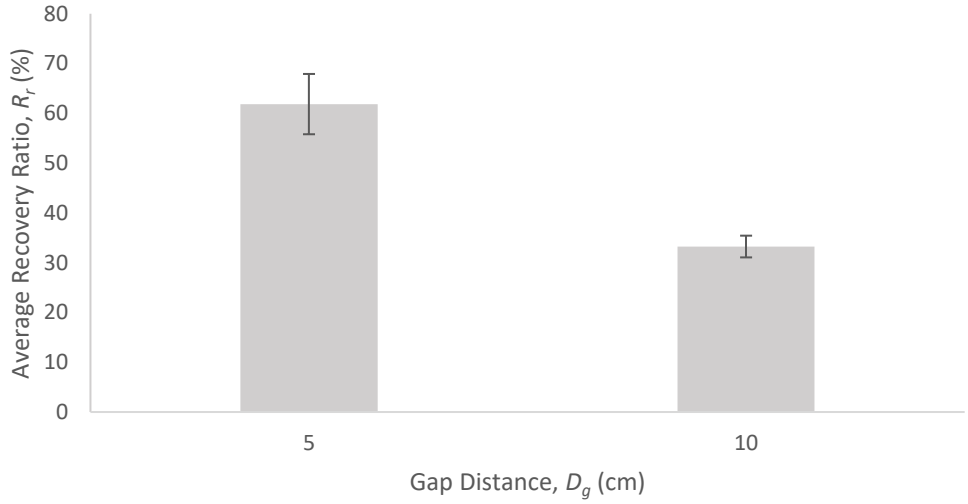

Figure 33- Change in Average Recovery Ratio over Varied Gap Distance at 15 kV

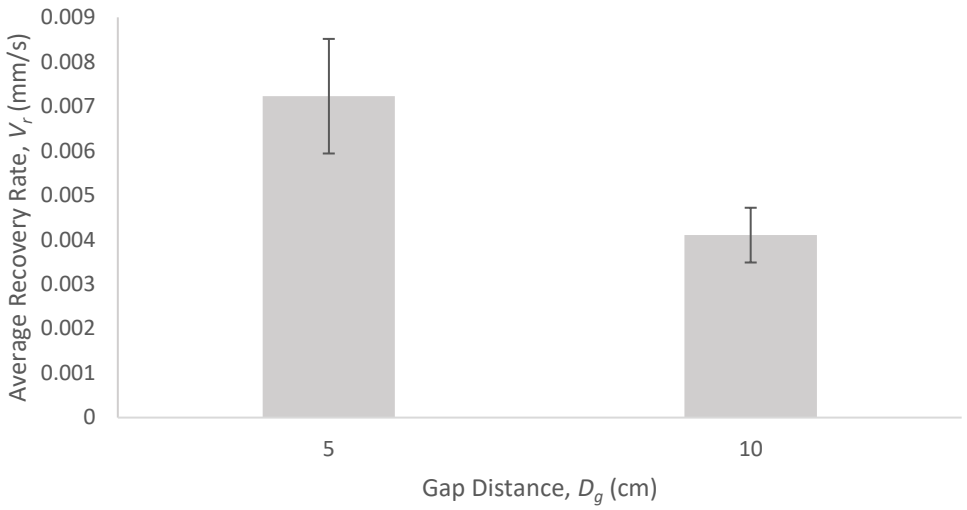

Figure 34- Change in Average Recovery Rate over Varied Gap Distance at 15 kV

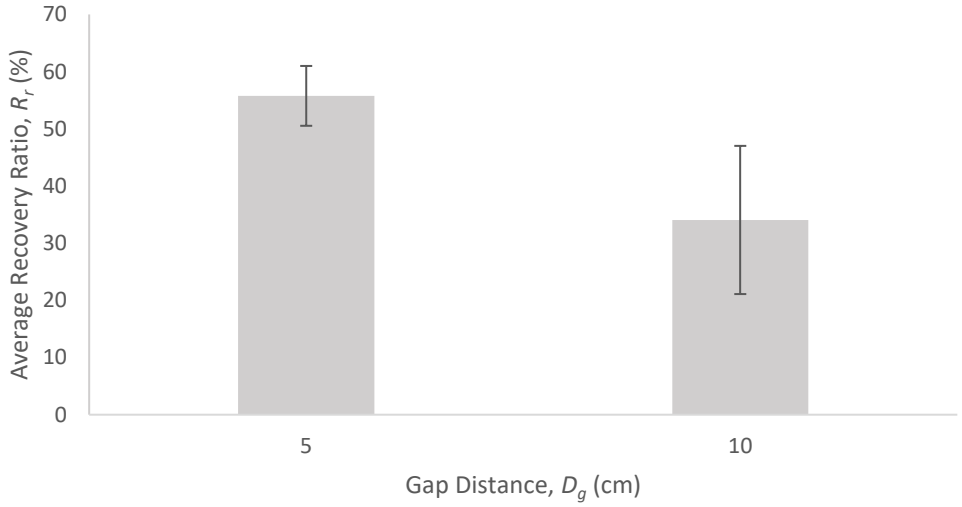

Figure 35- Change in Average Recovery Ratio over Varied Gap Distance at 20 kV

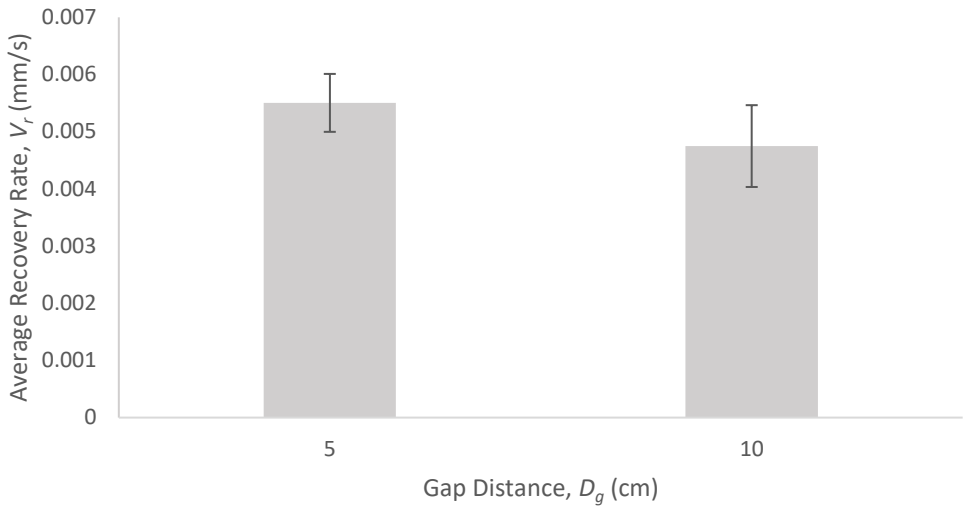

Figure 36- Change in Average Recovery Rate over Varied Gap Distance at 20 kV

Table 15- Maximum and Minimum Recovery Ratio and Recovery Rate with Constant Applied Voltage and Variable Gap Distance

Constant Voltage (kV)	Maximum Recovery Ratio Change (%)	Minimum Recovery Ratio Change (%)	Maximum Recovery Rate Change (mm/s)	Minimum Recovery Rate Change (mm/s)
15	36.8	20.4	0.00503	0.00122
20	39.9	3.51	0.00198	-0.000466

As noted, in contrast to the lack of readily apparent change in either of the shape memory parameters when the applied voltage was varied at a constant spinning gap distance, apparent change was seen when the spinning gap distance was varied at constant applied voltage. In particular, when a constant voltage of 15 kV was applied, varying the spinning gap distance from 5 cm to 10 cm resulted in an apparent reduction in both the recovery ratio and the recovery rate. When the voltage was held constant at 20 kV, an apparent reduction was found in the recovery ratio, but no such reduction was apparent in the recovery rate. Again, the direct root cause for a change being found here and not in the case when the applied voltage was varied at constant spinning gap distance is attributed to the larger change in the magnitude of the electrical field strength when the spinning gap distance was varied at constant applied voltage vs. when the voltage was varied at constant spinning gap distance.

3.3.2 Effect of Fiber Diameter/Mat Morphology on Shape Memory Properties

3.3.2.1 Effect of Fiber Diameter/Mat Morphology on Recovery Ratio

As was the case with the mechanical properties of the generated mats, an apparent reduction in the recovery ratio is seen to occur when the gap distance is varied at constant applied voltage, resulting in an apparent increase in the diameter of the fibers which make up the mats, while no change can be concluded to occur when the applied voltage was varied at constant gap distance, and as discussed above, this is believed to be due to the lower change in the electrostatic forces applied on the polymer jet when the voltage is varied at constant spinning gap distance than when the spinning gap distance is varied at constant voltage.

The first major difference between the generated mats is in the fiber diameters seen in the generated mats. As discussed previously, for the solution spun shape memory polymer mats, the literature reports mostly sub micrometer fiber diameters in solution electrospun polyurethane shape memory polymers [92],[93], [98], [103], with the largest reports found being in the sub 3 micron range [92], [93], [97]. In contrast, the smallest fibers found in this work where found to be 28.4± 6.8 μm and ranged to as large as 73.6 ± 18.9 μm. As noted previously, the work of Budun et al. noted an increase in the recovery ratio with increased diameter, but this was also accompanied by a more amorphous structure in their fibers [92]. While our fibers generated here are larger than the largest reported in Budun et al.'s work, they do not share the amorphous structure [92], which may indicate that the amorphous structure had more of an impact on the shape recovery properties than the fiber diameter in Budun et al.'s case [92]. It is believed that the cause of the apparent reduction in the recovery ratio when the gap distance was increased at constant applied voltage can be attributed to the apparent increase in the fiber diameter of the generated fibers, which likewise indicates that less stretching occurred in the polymeric jet during the spinning process. As noted previously, the effect of the electrospinning process to cause an elongation and orientation of the polymeric chains has been noted in the present literature [99], [182], [183], and this orientation has been noted to increase the recovery effect in melt-spun and drawn shape memory polymer [185] and in solution electrospun shape memory polymers [99]. The results seen here from the variation of the spinning parameters appear to align with these previous observations.

In particular, the apparent increase in the diameter when the spinning gap distance was increased from 5 cm to 10 cm indicates a lower amount of elongation of the polymer jet during the spinning proccess, and according to Greenfeld, Sui and Wagner, this would be indicative of less orientation in the molecular structure of the generated fibers [182]. Thus, this would then correlate to a reduction in the recovery ratio [99], [185], which can be seen to appear to occur based on the average values presented in Figure 33 and Figure 35. It is noted that this same effect cannot be concluded to be occurring when the voltage was varied at a constant gap distance of 5 cm, even though an apparent decrease in the diameter of the produced fibers was seen, as presented in Figure 12. It is believed that in this case that the increase in the elongation of polymer chains which came with the apparent decrease in the fiber diameter seen was likely not of a large enough magnitude in order to see significant change in the recovery ratio, whereas the larger reduction in this elongation/ apparent increase in diameter seen in the case of the varying spinning gap distance does produce enough of a magnitude change in order to see this effect. This is similar to the results seen with respect to the Young's modulus and yield strength, where it was believed that the elongation in the fibers was not of a high enough magnitude in order for the polymer chain alignment to have a significant effect on either of the mechanical properties.

3.3.2.2 Effect of Fiber Diameter/Mat Morphology on the Recovery Rate

In terms of the overall rate of recovery of the mats, as is the case with the recovery ratio, it is believed that the changes seen in the recovery rate with varying of the spinning parameters is due to the change in the elongation and orientation of the molecular makeup of the polymer due to the variation in the forces being placed on the polymer jet as the spinning parameters are varied, which can be seen physically through the apparent change in the fiber diameter. Nissenbaum, Greenfeld and Wagner reported a lower relaxation time constant in the case of solution electrospun shape memory polymer versus the shape memory polymer in bulk form [183], and they attributed this to less entanglements in the polymer chains of the electrospun material due to the elongation occurring during the spinning process [183]. It is possible that this phenomena is what is occurring to cause the apparent change in the recovery rate seen when the spinning gap distance was varied from 5 cm to 10 cm at 15 kV, as the decrease in the elongation which correlates with the apparent

increase in fiber diameter found due to this parameter change would, according to Nissenbaum, Greenfeld and Wagner, result in smaller reduction in entanglements and thus a longer recovery time [183]. If we consider the rate to be directly affected by the reduction in entanglements that comes with extension of the polymer chains [183], then at face value it would be expected to see an apparent change in the rate whenever we see an apparent change in the fiber diameter, as it can be correlated directly to the amount of stretching and elongation experienced by the polymer chains during the melt-electrospinning process. However two cases exist where we see an apparent change in the fiber diameter, but no corresponding change in the recovery rate can be stated to be occurring, these being when the voltage was varied at a 5 cm constant gap distance, and when the voltage was held constant at 20 kV and the gap distance was varied from 5 cm to 10 cm. In order to obtain a deeper understanding of the reasoning for this apparent discrepancy from what would be expected in general, a closer look into the change in the average fiber diameter in the other cases of apparent change in the fiber diameter without a corresponding apparent change in the recovery rate is needed, with this being contrasted with the particular case seen above.

In order to establish possible variations that occur in the other cases where apparent diameter change was seen, but no change in the recovery rate could be concluded, both the average change in the fiber diameter and the magnitude of the found fiber diameters is examined. First looking at the one case where the apparent change in the recovery rate was found (15 kV, with 5 cm-10 cm gap shift), an average diameter change of 25.6 μm is seen (fiber diameters varying from 48.0 ± 6.2 μm to 73.6 ± 18.9 μm). In the other two cases of apparent diameter change, at 5 cm constant gap distance with varied voltage, and a 20 kV constant voltage with varied gap distance, we see a change in the average fiber diameter of 19.6 μm (fiber diameters varying from 48.0 ± 6.2 μm to 28.4 ± 6.8 μm) and 28.1 μm (fibers diameters varying from 28.4 ± 6.8 μm to 56.5 ± 16.0 μm) respectively. These magnitudes of change are all quite close to one another, and in this case it would thus not appear that the magnitude of the diameter change is of itself having a major impact on the unexpected effect on the recovery rate. In contrast, more variation is seen when the actual average magnitudes of the fiber diameter are examined at each of these spinning parameter settings. At the 15 kV varied gap distance level, the lower recovery rate is found at an average fiber diameter of 73.6 ± 18.9 μm, while the higher level is found at an average fiber diameter of 48.0 ± 6.2 μm. In terms of the apparent diameter change at the 5 cm constant gap distance with varied voltage, the low recovery rate was found at an average fiber diameter of 28.4 ± 6.8 μm,

and the high recovery rate was found at an average fiber diameter of 48.0 ± 6.2 μm. Finally, in the 20 kV constant voltage with varied gap distance case, the high recovery rate was seen at an average fiber diameter of 28.4 ± 6.8 μm, and the low recovery rate was found at an average fiber diameter of 56.5 ± 16.0 μm. It is noted that in the two cases with only apparent changes in the fiber diameter, no pattern is seen with respect to the recovery rate. The obvious difference between the two cases where apparent change in the diameter was found without a corresponding apparent change in the recovery rate, and the case where both are seen is in the upper magnitude of the fiber diameter. In the two cases where only a significant change in the fiber diameter is seen the maximum average fiber diameter are at a similar level (48.0 ± 6.2 μm and 56.5 ± 16.0 μm), while the case where there was an apparent change in the recovery rate and the fiber diameter had an upper fiber diameter higher than either of these, at 73.6 ± 18.9 μm. It is likely that, with the correlation between the stretch in the polymer chains and the fiber diameter, that some critical value of diameter, as discussed by Greenfeld, Sui and Wagner with relation to Young's modulus in electrospun mats [182], is present with regards to the marked reduction in the recovery rate due to higher levels of chain entanglement [183]. It is believed that this is the most likely cause for this apparent discrepancy here, but further experimentation would be necessary to confirm this conclusion.

Chapter 4 Conclusion and Future Works

In the course of this work, non-woven shape memory polyurethane mats composed of MM 4520 thermoplastic polyurethane where generated utilizing the melt-electrospinning process. In the course of the study, the effect of the variation of the spinning gap distance and the applied voltage on the properties of the final non-woven mats were investigated. The spinning gap distance was investigated at a low and high level of 5 cm and 10 cm respectively, and the applied voltage was investigated at a low and high level of 15 kV and 20 kV respectively.

The morphology of both the non-woven mats themselves and the individual fibers which make up the mats were investigated at all four parameter combinations through the use of scanning electron microscopy. It was found that in all cases, the fibers produced where generally smooth uniform fibers with no beading present in any of the samples. In regards to the surface of the generated fibers, some imperfections where seen on fibers generate at the 5 cm spinning gap distance, and these were attributed to the cooling process. When examining the effect of varying the spinning parameter on the morphological structure of the mats, it was seen that when the applied voltage was varied from 15 kV to 20 kV while the spinning gap distance was held constant, the structure of the mats underwent an increase in the intertwined and coiled nature of the fiber structure at the 5 cm level, but a large change was not seen at the10 cm level. When the applied voltage was held constant and the spinning gap distance was varied from 5 cm to 10 cm, a marked decrease in winding and coiling was seen in the fibers at both the 15 kV and 20 kV levels. It is believed that the more pronounced structural changes seen when the spinning gap distance was increased versus when the applied voltage was increased can be ascribed to the larger change in the electrical field strength seen when the spinning gap distance was varied versus when the applied voltage was varied.

Along with the morphology the average fiber diameter of the mats generated at each of the 4 parameter combinations were investigated. A maximum average fiber diameter of 73.6 ± 18.9 μm was found when the applied voltage was set to 15 kV and the spinning gap distance was set to 10 cm, while a minimum average fiber diameter of 28.4 ± 6.8 μm was found when the applied

voltage was set to 20 kV and the spinning gap distance was set to 5 cm. In terms of trends in the fiber diameter with varying spinning parameters, it was found that, for the range of parameters selected, increasing the applied voltage while the spinning gap distance was held constant resulted in an apparent decrease in the average fiber diameter at a 5 cm spinning gap distance, but no change at a 10 cm spinning gap distance could be concluded to be occurring. When the spinning gap distance was varied from 5 cm to 10 cm, an apparent increase in the fiber diameter was found at constant voltages of both 15 kV and 20 kV. In general, it is believed that the change in the fiber diameter at the investigate parameter combinations is due to the change in the electrical field strength of the melt-electrospinning system. When the voltage was increased at the 5 cm spinning gap distance, a corresponding apparent decrease in the fiber diameter occurred due to the larger electrostatic force placed on the polymer jet by the larger electrical field strength. In the case of the 10 cm spinning gap distance, the change seen in the electrical field strength was not of a large enough magnitude in order to achieve an a decrease in the average fiber diameter. Likewise, when the spinning gap distance was increased at constant voltage levels, the magnitude of the decrease in the electrical field strength was large enough in both cases to induce an apparent increase in the fiber diameter.

The mechanical properties, specifically the Young's modulus and yield strength were investigated by traditional tensile testing. A maximum average Young's modulus of 14.2 ± 4.0 MPa was found when the mats were spun at a 5 cm spinning gap distance and a 15 kV applied voltage, while the minimum average Young's modulus of 8.38 ± 2.41 MPa was found when the mats where spun at a 10 cm spinning gap distance and a 15 kV applied voltage. In terms of the effect of the variation of the two selected spinning parameters, it was found that conclusions on the effect on the Young's modulus occurred over any of the investigated parameter ranges could not be reached. This lack of apparent effect of the spinning parameters on the value of the Young's modulus was believed to be due to the diameter range of the fibers which made up the non-woven mats (28.4 ± 6.8 μm to 73.6 ± 18.9 μm) being above a critical value where an effect on the Young's modulus would occur due to polymer chain alignment and stretching due to the melt-electrospinning process. As well, it was believed that the morphological structure of the mats which was found to change with the variation of the spinning parameters did not affect the Young's modulus of the mats as a number of fibers would always be under direct tensile loading throughout the elastic region. In terms of the yield strength, a maximum average value of 4.27 ± 0.74 MPa,

which resulted from a spinning gap distance of 5 cm and an applied voltage of 15 kV was found, while the minimum average yield strength was found to be 2.13 ± 0.23 MPA, achieved when the spinning process occurred at a spinning gap distance of 10 cm and an applied voltage of 15 kV. When the applied voltage was varied with the spinning gap distance held constant at the two selected levels, no conclusion on the effect on the yield strength could be made. In contrast, when the spinning gap distance was varied from 5 cm to 10 cm with the voltage level held constant, an apparent change in the yield strength was seen at both the 15 kV and 20 kV level, with an apparent decrease in the yield strength being seen in both cases. As was the case with the Young's modulus, the microstructure of the polymer was not believed to be having a major effect on yield strength. It was believed that the decrease when the gap distance was increased from 5 cm to 10 cm was due to the change in the macro structure of the mats from a more twisted and overlapping fiber structure to a structure made of straighter, less intertwined fibers. The decrease was believed to be due to the fact that as the material was loaded, in the more random structure at 5 cm, new fiber were able to unwind and being taking the load as other fibers yielded, while the straighter structure provided less opportunity for new fibers to come under load, causing the bulk mat to completely yield earlier, and thus resulting in a lower yield strength.

Finally, the shape memory properties of the melt-electrospun shape memory polymer mats where investigated at the various spinning parameters. In particular, the recovery ratio and the recovery rate of the non-woven mats where examined at each of the four parameter combinations. In the case of the recovery ratio, a maximum average value of 61.9 ± 6.1 % was found when the mat was generated at a spinning gap distance of 5 cm and an applied voltage of 15 kV, while the minimum average recovery ratio was found to be 33.2 ± 2.2 %, which was achieved when the spinning gap distance was set to 10 cm, and the applied voltage was set to 15 kV. When the effect of the variation of the spinning parameters on the recovery ratio was examined, it was found that with the variation of the applied voltage from 15 kV to 20 kV at constant spinning gap distances of 5 cm and 10 cm no conclusion on the effect on the recovery ratio could be made, but when the spinning gap distance was varied from 5 cm to 10 cm at constant applied voltages of 15 kV and 20 kV an apparent decrease in the recovery ratio was found in both cases. The cause of the apparent change in the recovery ratio was attributed to the change in the magnitude of the electrical field strength which was caused by the variation of the spinning parameters. When the spinning gap distance was varied, a larger change in the electrical field strength occurred than when the applied

voltage was varied. This resulted in the variation of the spinning gap distance causing an apparent change in the recovery ratio, while variation of the applied voltage level did not. The structural reason for this change is believed to be due to the change in the alignment and stretching of the polymer chains with increasing or decreasing electrical field strength. The variation of the applied voltage did not cause a large enough variation of the magnitude in the level of chain alignment and stretching in order to cause any change, while the variation in the spinning gap distance did, specifically a decrease in the magnitude of alignment. In the case of the recovery rate, a maximum average recovery rate of 0.00723 ± 0.00129 mm/s was found to occurred when the mats were generated at a spinning gap distance of 5 cm and an applied voltage of 15 kV, while the minimum average recovery rate was found to be 0.00410 ± 0.00062 mm/s, which was achieved from a mat generated at a spinning gap distance of 10 cm and a spinning gap distance of 15 kV. It contrast to the recovery ratio, when the effect of varying the spinning parameters on the recovery rate was examined, it was found that only varying the spinning gap distance from 5 cm to 10 cm at the 15 kV applied voltage level caused an apparent decrease in the total recovery rate. It is again believed that the change seen was due to the change in the magnitude of the electrical field strength, which correlated to a change in the degree of polymeric chain alignment, and specifically the level of entanglement of the polymer chains. The limited effect was believed to be due to the fact that the magnitude of the polymer chain entanglement, which was correlated with the fiber diameter did not reach a critical level where it had an effect in the cases other than the variation of the spinning gap distance at the 15 kV level.

It is believed that the work presented here has given a good first step in the characterization of the behavior of melt-electrospun shape memory polymer non-woven materials. Future work to complete this full characterization of randomly distributed non-woven mats would include an investigation of the fixity ratio (R_f) in order to develop an understanding of the materials ability to maintain the programed shape prior to the recovery process being initiated. As well, a more detailed parameter study involving a larger number of investigated melt-electrospinning parameters and a higher number of levels at each parameter should be pursued in order to obtain a more detailed understanding of the entire process as well as if the variation of the parameters result in higher order effects. This study should also include a statistical analysis of the variation caused by the study of the various spinning parameters. This will allow better insight into the apparent trends seen in this work with regards to the investigated properties.

In addition to this continued work on randomly distributed materials, it is suggested by the author that inquiry into the mechanical and shape memory behaviour of aligned melt-electrospun shape memory polymer fibers be conducted. This future inquiry should include both the general mechanical and shape memory characterization for the fully aligned shape memory polymer fiber mats, along with an investigation into how the alignment of the fibers is effected by the variation of the rotational velocity of the collection drum, and how these varying degrees of alignment effect the noted properties of the non-woven mats.

Finally, future work should also include investigation into the practical applications of these non-woven materials, in the randomly distributed and aligned variations. Possible areas of inquiry may include biomedical applications, textiles, and filtration. Development of real world uses for these materials will allow for the preliminary work found in this study to reach a fuller completion in practical application outside of the laboratory environment.

Bibliography

[1] L. Sun *et al.*, "Stimulus-responsive shape memory materials: A review," *Materials and Design*, vol. 33, no. 1. Elsevier, pp. 577–640, 01-Jan-2012.

[2] C. Liu, H. Qin, and P. T. Mather, "Review of progress in shape-memory polymers," *J. Mater. Chem.*, vol. 17, no. 16, pp. 1543–1558, 2007.

[3] C. Liang, C. A. Rogers, and E. Malafeew, "Investigation of Shape Memory Polymers and Their Hybrid Composites," *J. Intell. Mater. Syst. Struct.*, vol. 8, no. 4, pp. 380–386, 1997.

[4] H. Tobushi, S. Hayashi, and S. Kojima, "Mechanical properties of shape memory polymer of polyurethane series. (Basic characteristics of stress-strain-temperature relationship)," *JSME Int. Journal, Ser. 1 Solid Mech. Strength Mater.*, vol. 35, no. 3, pp. 296–302, 1992.

[5] H. TOBUSHI, S. HAYASHI, and S. KOJIMA, "Uniaxial Creep Deformation of Shape Memory Polymer of Polyurethane Series," *Trans. Japan Soc. Mech. Eng. Ser. A*, vol. 58, no. 556, pp. 2434–2439, 1992.

[6] H. TOBUSHI, S. HAYASHI, and S. KOJIMA, "Cyclic Deformation of shape Memory Polymer of Polyurethane Series Subjected to Loading at Low Temperature," *Trans. Japan Soc. Mech. Eng. Ser. A*, vol. 58, no. 554, pp. 1889–1894, 1992.

[7] H. TOBUSHI, S. HAYASHI, and S. KOJIMA, "Cyclic Deformation Properties of Shape Memory Polymer of Polyurethane Series.," *Trans. Japan Soc. Mech. Eng. Ser. A*, vol. 58, no. 554, pp. 1883–1888, 1992.

[8] S. Echigo *et al.*, "Development of a new transvenous patent ductus arteriosus occlusion technique using a shape memory polymer," *ASAIO Trans*, vol. 36, no. 3. pp. M195-8, 1990.

[9] Y. Ujihira, H.-L. Li, and K. Ito, "Free Volume Study on Three Types of Shape Memory Polymers by Positron Annihilation," *Acta Phys. Pol. A*, vol. 95, no. 4, pp. 677–682, Apr. 1999.

[10] H.-L. LI, K. ITO, Y. UJIHIRA, A. NANASAWA, and T. IWAMOTO, "Variation of Free Volume Size, Size Distribution, and Numerical Concentration in Shape Memory Polymer-Polystyrene Polybutadiene Copolymer-with Temperature, Studied by Positron Annihilation Lifetime Technique.," *KOBUNSHI RONBUNSHU*, vol. 55, no. 8, pp. 448–455, 1998.

[11] H. Tobushi, S. Hayashi, and P. Lin, "Deformation Properties of Shape Memory Polymers of Polyurethane Series.," *Trans. Japan Soc. Mech. Eng. Ser. A*, vol. 60, no. 575, pp. 1676–1681, 1994.

[12] H. TOBUSHI, S. HAYASHI, H. HARA, E. YAMADA, and T. HASHIMOTO, "Cyclic Properties of Energy Dissipation and Storage in a Film Made of Shape Memory Polymer of the Polyurethane Series," *Trans. Japan Soc. Mech. Eng. Ser. A*, vol. 63, no. 613, pp. 1986–1992, 1997.

[13] H. Tobushi, T. Hashimoto, S. Hayashi, and E. Yamada, "Thermomechanical Constitutive Modeling in Shape Memory Polymer of Polyurethane Series," *J. Intell. Mater. Syst. Struct.*, vol. 8, no. 8, pp. 711–718, Aug. 1997.

[14] Y. Kagami, J. P. Gong, and Y. Osada, "Shape memory behaviors of crosslinked copolymers containing stearyl acrylate," *Macromol. Rapid Commun.*, vol. 17, no. 8, pp. 539–543, Aug. 1996.

[15] H. Tobushi, T. Hashimoto, N. Ito, S. Hayashi, and E. Yamada, "Shape Fixity and Shape Recovery in a Film of Shape Memory Polymer of Polyurethane Series," *J. Intell. Mater. Syst. Struct.*, vol. 9, no. 2, pp. 127–136, 1998.

[16] H. TOBUSHI, S. HAYASHI, A. IKAI, and H. HARA, "Basic Deformation Properties of a Polyurethane-Series Shape Memory Polymer Film," *Trans. Japan Soc. Mech. Eng. Ser. A*, vol. 62, no. 594, pp. 576–582, 1996.

[17] H. Tobushi, H. Hara, E. Yamada, and S. Hayashi, "Thermomechanical properties in a thin film of shape memory polymer of polyurethane series," *Smart Mater. Struct.*, vol. 5, no. 4, pp. 483–491, 1996.

[18] H. TOBUSHI, S. HAYASHI, A. IKAI, H. HARA, and E. YAMADA, “Creep and Stress Relaxation in a Film of Shape Memory Polymers of Polyurethane Series.,” *Trans. Japan Soc. Mech. Eng. Ser. A*, vol. 62, no. 599, pp. 1619–1625, 1996.

[19] W. M. Sokolowski, A. B. Chmielewski, S. Hayashi, and T. Yamada, “Cold hibernated elastic memory (CHEM) self-deployable structures,” in *Smart Structures and Materials 1999: Electroactive Polymer Actuators and Devices*, 1999, vol. 3669, no. May, pp. 179–185.

[20] J. D. Chiodo, E. H. Billett, and D. J. Harrison, “Active disassembly using shape memory polymers for the mobile phone industry,” in *Proceedings of the 1999 IEEE International Symposium on Electronics and the Environment (Cat. No.99CH36357)*, 1999, pp. 151–156.

[21] M. Wang and L. Zhang, “Recovery as a measure of oriented crystalline structure in poly(ether ester)s based on poly(ethylene oxide) and poly(ethylene terephthalate) used as shape memory polymers,” *J. Polym. Sci. Part B Polym. Phys.*, vol. 37, no. 2, pp. 101–112, Jan. 1999.

[22] F. Li, W. Zhu, X. Zhang, C. Zhao, and M. Xu, “Shape memory effect of ethylene-vinyl acetate copolymers,” *J. Appl. Polym. Sci.*, vol. 71, no. 7, pp. 1063–1070, Feb. 1999.

[23] D. A. Russell, S. Hayashi, and T. Yamada, “The Potential Uses of Shape Memory Film in Clothing,” in *Proceedings of Techtextile Symposium 1999*, 1999.

[24] J. D. Chiodo, E. H. Billett, and D. J. Harrison, “Preliminary investigations of active disassembly using shape memory polymers,” in *Proceedings First International Symposium on Environmentally Conscious Design and Inverse Manufacturing*, 1999, pp. 590–596.

[25] B. Z. Jang and Z. J. Zhang, “Thermally- and Phase Transformation-Induced Volume Changes of Polymers for Actuator Applications,” *J. Intell. Mater. Syst. Struct.*, vol. 5, no. 6, pp. 758–763, Nov. 1994.

[26] R. P. Kusy and J. Q. Whitley, “Thermal characterization of shape memory polymer blends for biomedical implantations,” *Thermochim. Acta*, vol. 243, no. 2, pp. 253–263, Sep. 1994.

[27] A. Lendlein, A. M. Schmidt, and R. Langer, “AB-polymer networks based on oligo(ε-caprolactone) segments showing shape-memory properties,” *Proc. Natl. Acad. Sci.*, vol. 98, no. 3, pp. 842–847, 2001.

[28] A. Lendlein and R. Langer, “Biodegradable, Elastic Shape-Memory Polymers for Potential Biomedical Applications,” *Science (80-.).*, vol. 296, no. 5573, pp. 1673–1676, 2002.

[29] A. Lendlein, M. Behl, B. Hiebl, and C. Wischke, “Shape-memory polymers as a technology platform for biomedical applications,” *Expert Rev. Med. Devices*, vol. 7, no. 3, pp. 357–379, May 2010.

[30] D. Rickert *et al.*, “In vitro cytotoxicity testing of AB-polymer networks based on oligo(ϵ-caprolactone) segments after different sterilization techniques,” *J. Biomed. Mater. Res. Part B Appl. Biomater.*, vol. 67B, no. 2, pp. 722–731, 2003.

[31] M. Bertmer, A. Buda, I. Blomenkamp-Höfges, S. Kelch, and A. Lendlein, “Biodegradable Shape-Memory Polymer Networks: Characterization with Solid-State NMR,” *Macromolecules*, vol. 38, no. 9, pp. 3793–3799, 2005.

[32] J. Zotzmann, M. Behl, D. Hofmann, and A. Lendlein, “Reversible Triple-Shape Effect of Polymer Networks Containing Polypentadecalactone- and Poly(ε-caprolactone)-Segments,” *Adv. Mater.*, vol. 22, no. 31, pp. 3424–3429, 2010.

[33] A. Lendlein, “16 - Tailor-made intelligent polymers for biomedical applications,” in *Smart Fibres, Fabrics and Clothing*, X. Tao, Ed. Woodhead Publishing, 2001, pp. 278–290.

[34] M. Behl and A. Lendlein, “Shape-memory polymers,” *Mater. Today*, vol. 10, pp. 20–28, 2007.

[35] G. . Monkman, “Advances in shape memory polymer actuation,” *Mechatronics*, vol. 10, no. 4–5, pp. 489–498, Jun. 2000.

[36] K. Gall, M. Mikulas, N. A. Munshi, F. Beavers, and M. Tupper, “Carbon Fiber Reinforced Shape Memory Polymer Composites,” *J. Intell. Mater. Syst. Struct.*, vol. 11, no. 11, pp. 877–886, Nov. 2000.

[37] K. Gall, “Shape memory polymer nanocomposites,” *Acta Mater.*, vol. 50, no. 20, pp. 5115–5126, Dec. 2002.

[38] J.-N. Zhang *et al.*, “Microfiber SMPU film affords quicker shape recovery than the bulk one,” *Mater. Lett.*, vol. 65, no. 23–24, pp. 3639–3642, Dec. 2011.

[39] L. Xue, S. Dai, and Z. Li, “Biodegradable shape-memory block co-polymers for fast self-expandable stents,” *Biomaterials*, vol. 31, no. 32, pp. 8132–8140, Nov. 2010.

[40] J. D. Chiodo, D. J. Harrison, and E. H. Billett, “An initial investigation into active disassembly using shape memory polymers,” *Proc. Inst. Mech. Eng. Part B J. Eng. Manuf.*, vol. 215, no. 5, pp. 733–741, May 2001.

[41] D. M. Fatiha El Feninat, Gaetan Laroche, Michel Fiset, “Shape Memory Materials for Biomedical Applications,” *Adv. Eng. Mater.*, vol. 4, no. 3, pp. 91–104, 2002.

[42] S. Chen, J. Hu, C. Yuen, and L. Chan, “Novel moisture-sensitive shape memory polyurethanes containing pyridine moieties,” *Polymer (Guildf).*, vol. 50, no. 19, pp. 4424–4428, Sep. 2009.

[43] D. J. Maitland, M. F. Metzger, D. Schumann, A. Lee, and T. S. Wilson, “Photothermal properties of shape memory polymer micro-actuators for treating stroke,” *Lasers Surg. Med.*, vol. 30, no. 1, pp. 1–11, Jan. 2002.

[44] X.-J. Han *et al.*, “pH-Induced Shape-Memory Polymers,” *Macromol. Rapid Commun.*, vol. 33, no. 12, pp. 1055–1060, Jun. 2012.

[45] I. T. Garces, S. Aslanzadeh, Y. Boluk, and C. Ayranci, “Effect of moisture on shape memory polyurethane polymers for extrusion-based additive manufacturing,” *Materials (Basel).*, vol. 12, no. 2, p. 244, 2019.

[46] R. Bhattacharyya, C. V. Di Leo, C. Floerkemeier, S. Sarma, and L. Anand, “RFID Tag Antenna Based Temperature Sensing Using Shape Memory Polymer Actuation,” *Proc. IEEE Sensors*, pp. 2363–2368, 2010.

[47] T. D. Dao, N. S. Goo, and W. R. Yu, “Blocking force measurement of shape memory polymer composite hinges for space deployable structures,” *J. Intell. Mater. Syst. Struct.*, vol. 29, no. 18, pp. 3667–3678, Sep. 2018.

[48] M. J. Jo *et al.*, “Preparation of Epoxy Shape Memory Polymers for Deployable Space Structures Using Flexible Diamines,” *Fibers Polym.*, vol. 19, no. 9, pp. 1799–1805, 2018.

[49] L. S. and F. Q. and D. Bellisario, “Shape memory composite antennas for space applications,” *IOP Conf. Ser. Mater. Sci. Eng.*, vol. 161, no. 1, p. 12066, 2016.

[50] J. H. Jang *et al.*, “Durability of carbon fiber reinforced shape memory polymer composites in space,” in *Behavior and Mechanics of Multifunctional Materials and Composites 2016*, 2016, vol. 9800, p. 98000I.

[51] D. Bergman and B. Yang, “An Analytical Shape Memory Polymer Composite Beam Model for Space Applications,” *Int. J. Struct. Stab. Dyn.*, vol. 16, no. 02, p. 1450093, Jan. 2015.

[52] R. Zhang, X. Guo, Y. Liu, and J. Leng, “Theoretical analysis and experiments of a space deployable truss structure,” *Compos. Struct.*, vol. 112, pp. 226–230, 2014.

[53] J.-H. Roh, H.-J. Kim, and J.-S. Bae, “Shape memory polymer composites with woven fabric reinforcement for self-deployable booms,” *J. Intell. Mater. Syst. Struct.*, vol. 25, no. 18, pp. 2256–2266, Dec. 2014.

[54] Q. Fabrizio, S. Loredana, and S. E. Anna, “Shape memory epoxy foams for space applications,” *Mater. Lett.*, vol. 69, pp. 20–23, 2012.

[55] D. Bergman, B. Yang, G. Davis, and H. Fang, “Modeling and Quasi-Static Analysis of a Shape Memory Polymer Cantilever Beam for Space Applications,” in *53rd AIAA/ASME/ASCE/AHS/ASC Structures, Structural Dynamics and Materials Conference*, American Institute of Aeronautics and Astronautics, 2012.

[56] A. Y. N. Sofla, S. A. Meguid, K. T. Tan, and W. K. Yeo, “Shape morphing of aircraft wing: Status and challenges,” *Mater. Des.*, vol. 31, no. 3, pp. 1284–1292, 2010.

[57] O. T. and M. P. and R. D. and J. S. and T. J. and R. L. and D. Gardner, “A shape memory polymer concrete crack closure system activated by electrical current,” *Smart Mater. Struct.*, vol. 27, no. 7, p. 75016, 2018.

[58] H. Luo *et al.*, “Multi-stimuli triggered self-healing of the conductive shape memory polymer composites,” *Pigment Resin Technol.*, vol. 47, no. 1, pp. 1–6, 2018.

[59] M. Invernizzi, S. Turri, M. Levi, and R. Suriano, “4D printed thermally activated self-healing and shape memory polycaprolactone-based polymers,” *Eur. Polym. J.*, vol. 101, pp. 169–176, Apr. 2018.

[60] L. Wang *et al.*, “Shape memory composite (SMC) self-healing coatings for corrosion protection,” *Prog. Org. Coatings*, vol. 97, pp. 261–268, 2016.

[61] Y. Q. Yougoubare, I. J. Okoro, and S.-S. Pang, “Effects of Programming Temperature on the Efficiency of Self-Healing Polymers,” in *Proceedings of the ASME 2012 Pressure Vessels & Piping Conference PVP2012 Volume 6: Materials and Fabrication, Parts A and B*, 2012, no. 55058, pp. 239–242.

[62] M. H. Malakooti and H. A. Sodano, “Fracture Modeling of an Embedded Crack in Self-Healing Polymers,” in *ASME 2012 Conference on Smart Materials, Adaptive Structures and Intelligent Systems, SMASIS 2012*, 2012, no. 1, pp. 149–155.

[63] J. Nji and G. Li, “A self-healing 3D woven fabric reinforced shape memory polymer composite for impact mitigation,” *Smart Mater. Struct.*, vol. 19, no. 3, p. 35007, 2010.

[64] G. Li and D. Nettles, “Thermomechanical characterization of a shape memory polymer based self-repairing syntactic foam,” *Polymer (Guildf).*, vol. 51, no. 3, pp. 755–762, 2010.

[65] X. Xiao, T. Xie, and Y.-T. Cheng, “Self-healable graphene polymer composites,” *J. Mater. Chem.*, vol. 20, no. 17, pp. 3508–3514, 2010.

[66] G. Li and N. Uppu, “Shape memory polymer based self-healing syntactic foam: 3-D confined thermomechanical characterization,” *Compos. Sci. Technol.*, vol. 70, no. 9, pp. 1419–1427, 2010.

[67] Q. Ge, A. Serjouei, H. J. Qi, and M. L. Dunn, “Thermomechanics of printed anisotropic shape memory elastomeric composites,” *Int. J. Solids Struct.*, vol. 102–103, pp. 186–199, 2016.

[68] M. Kang *et al.*, “Design of a shape memory composite(SMC) using 4D printing technology,” *Sensors Actuators A Phys.*, vol. 283, pp. 187–195, 2018.

[69] J. H. Kang, E. J. Siochi, R. K. Penner, and T. L. Turner, “Enhanced adhesive strength between shape memory polymer nanocomposite and titanium alloy,” *Compos. Sci. Technol.*, vol. 96, pp. 23–30, 2014.

[70] H. Lu, W. M. Huang, and J. Leng, “Functionally graded and self-assembled carbon nanofiber and boron nitride in nanopaper for electrical actuation of shape memory nanocomposites,” *Compos. Part B Eng.*, vol. 62, pp. 1–4, 2014.

[71] Q. Zhang, S. Song, J. Feng, and P. Wu, “A new strategy to prepare polymer composites with versatile shape memory properties,” *J. Mater. Chem.*, vol. 22, no. 47, pp. 24776–24782, 2012.

[72] Z. Wang, W. Song, L. Ke, and Y. Wang, “Shape memory polymer composite structures with two-way shape memory effects,” *Mater. Lett.*, vol. 89, pp. 216–218, 2012.

[73] G. P. Tandon, K. Goecke, K. Cable, and J. Baur, “Environmental Durability of Fabric-Reinforced Shape-Memory Polymer Composites,” *J. Intell. Mater. Syst. Struct.*, vol. 21, no. 14, pp. 1365–1381, Sep. 2010.

[74] J. N. Rodriguez *et al.*, “Opacification of Shape Memory Polymer Foam Designed for Treatment of Intracranial Aneurysms,” *Ann. Biomed. Eng.*, vol. 40, no. 4, pp. 883–897, Apr. 2012.

[75] K. Takashima, J. Rossiter, and T. Mukai, “McKibben artificial muscle using shape-memory polymer,” *Sensors Actuators A Phys.*, vol. 164, no. 1–2, pp. 116–124, Nov. 2010.

[76] E. M. Lee, K. Smith, K. Gall, B. D. Boyan, and Z. Schwartz, “Change in surface roughness by dynamic shape-memory acrylate networks enhances osteoblast differentiation,” *Biomaterials*, vol. 110, pp. 34–44, Dec. 2016.

[77] L. Yin, S. Wang, and S. Zuo, “Water-jet outer sheath with braided shape memory polymer tubes for upper gastrointestinal tract screening,” *Int. J. Med. Robot. Comput. Assist. Surg.*, vol. 14, no. 6, p. e1944, Dec. 2018.

[78] J. N. Rodriguez *et al.*, “Reticulation of low density shape memory polymer foam with an in vivo demonstration of vascular occlusion,” *J. Mech. Behav. Biomed. Mater.*, vol. 40, pp. 102–114, 2014.

[79] R. Kunkel *et al.*, “Synthesis and characterization of bio-compatible shape memory polymers with potential applications to endovascular embolization of intracranial aneurysms,” *J. Mech. Behav. Biomed. Mater.*, vol. 88, pp. 422–430, Dec. 2018.

[80] L.-F. Tseng, P. T. Mather, and J. H. Henderson, “A programmable shape-changing scaffold for regenerative medicine,” in *2012 38th Annual Northeast Bioengineering Conference (NEBEC)*, 2012, pp. 227–228.

[81] C. Wischke, A. T. Neffe, S. Steuer, and A. Lendlein, “Comparing techniques for drug loading of shape-memory polymer networks – effect on their functionalities,” *Eur. J. Pharm. Sci.*, vol. 41, no. 1, pp. 136–147, 2010.

[82] M. A. Zainal and M. S. M. Ali, “Wireless shape memory polymer microactuator for implantable drug delivery aplication,” in *2016 IEEE EMBS Conference on Biomedical Engineering and Sciences (IECBES)*, 2016, pp. 76–79.

[83] H. Chen, H. Xia, Y. Qiu, Z. Xu, and Q.-Q. Ni, “Smart composites of piezoelectric particles and shape memory polymers for actuation and nanopositioning,” *Compos. Sci. Technol.*, vol. 163, pp. 123–132, 2018.

[84] J. T. Cantrell, J. R. Van Hall, A. J. Young, and P. G. Ifju, “Experimental Characterization of Shape Fixity in Transversely Curved Unimorph Shape Memory Polymer Actuators,” in *Experimental and Applied Mechanics, Volume 4*, 2016, pp. 1–10.

[85] K. Ren, R. S. Bortolin, and Q. M. Zhang, “An investigation of a thermally steerable electroactive polymer/shape memory polymer hybrid actuator,” *Appl. Phys. Lett.*, vol. 108, no. 6, p. 062901, Feb. 2016.

[86] C. M. J. L. Lelieveld and K. M. B. Jansen, “Thermal–electric characterization and modelling of a smart composite structure for architectural applications,” *Smart Mater. Struct.*, vol. 23, no. 6, p. 65010, 2014.

[87] F. Auffinger, M. Fisher, and M. Maddux, “Shape memory polymer (SMP) actuation technology,” in *Sensors and Smart Structures Technologies for Civil, Mechanical, and Aerospace Systems 2010*, 2010, vol. 7647, p. 76473A.

[88] D. Jocić, “Polymer-Based Smart Coatings for Comfort in Clothing,” *Tekstilec*, vol. 59, no. 2, pp. 107–114, May 2016.

[89] M. Jahid *et al.*, “Fabric Coated with Shape Memory Polyurethane and Its Properties,” *Polymers (Basel).*, vol. 10, no. 6, p. 681, Jun. 2018.

[90] N. Bhardwaj and S. C. Kundu, “Electrospinning: A fascinating fiber fabrication technique,” *Biotechnology Advances*, vol. 28, no. 3. pp. 325–347, 2010.

[91] W. Cui, X. Li, S. Zhou, and J. Weng, “Investigation on process parameters of electrospinning system through orthogonal experimental design,” *J. Appl. Polym. Sci.*, vol. 103, no. 5, pp. 3105–3112, Mar. 2007.

[92] S. Budun, E. İşgören, R. Erdem, and M. Yüksek, “Morphological and mechanical analysis of electrospun shape memory polymer fibers,” *Appl. Surf. Sci.*, vol. 380, pp. 294–300, Sep. 2016.

[93] D. Kai *et al.*, “Elastic poly(ε -caprolactone)-polydimethylsiloxane copolymer fibers with shape memory effect for bone tissue engineering,” *Biomed. Mater.*, vol. 11, no. 1, p. 15007, 2016.

[94] J. Y. Ang, B. Q. Y. Chan, D. Kai, and X. J. Loh, “Engineering Porous Water-Responsive Poly(PEG/PCL/PDMS Urethane) Shape Memory Polymers,” *Macromol. Mater. Eng.*, vol. 302, no. 9, p. 1700174, 2017.

[95] J.-S. Ahn, W.-R. Yu, J. H. Youk, and H. Y. Ryu, “In situ temperature tunable pores of shape memory polyurethane membranes,” *Smart Mater. Struct.*, vol. 20, no. 10, p. 105024, 2011.

[96] L. F. Tseng, P. T. Mather, and J. H. Henderson, “Shape-memory-actuated change in scaffold fiber alignment directs stem cell morphology,” *Acta Biomater.*, vol. 9, no. 11, pp. 8790–8801, Nov. 2013.

[97] D. Il Cha, H. Y. Kim, K. H. Lee, Y. C. Jung, J. W. Cho, and B. C. Chun, “Electrospun nonwovens of shape-memory polyurethane block copolymers,” *J. Appl. Polym. Sci.*, vol. 96, no. 2, pp. 460–465, 2005.

[98] D. Kai *et al.*, “Biocompatible electrically conductive nanofibers from inorganic-organic shape memory polymers,” *Colloids Surfaces B Biointerfaces*, vol. 148, pp. 557–565, Dec. 2016.

[99] S. E. Chung, C. H. Park, W.-R. Yu, and T. J. Kang, “Thermoresponsive shape memory characteristics of polyurethane electrospun web,” *J. Appl. Polym. Sci.*, vol. 120, no. 1, pp. 492–500, 2011.

[100] W. Kuang and P. T. Mather, “A latent crosslinkable PCL-based polyurethane: Synthesis, shape memory, and enzymatic degradation,” *J. Mater. Res.*, vol. 33, no. 17, pp. 2463–2476, 2018.

[101] H. Zhuo, J. Hu, and S. Chen, “Electrospun polyurethane nanofibres having shape memory effect,” *Mater. Lett.*, vol. 62, no. 14, pp. 2074–2076, May 2008.

[102] J. Wang, A. Quach, M. E. Brasch, C. E. Turner, and J. H. Henderson, “On-command on/off switching of progenitor cell and cancer cell polarized motility and aligned morphology via a cytocompatible shape memory polymer scaffold,” *Biomaterials*, vol. 140, pp. 150–161, Sep. 2017.

[103] L. Tan, L. Gan, J. Hu, Y. Zhu, and J. Han, “Functional shape memory composite nanofibers with graphene oxide filler,” *Compos. Part A Appl. Sci. Manuf.*, vol. 76, pp. 115–123, Sep. 2015.

[104] A. H. Torbati, R. T. Mather, J. E. Reeder, and P. T. Mather, “Fabrication of a light-emitting shape memory polymeric web containing indocyanine green,” *J. Biomed. Mater. Res. Part B Appl. Biomater.*, vol. 102, no. 6, pp. 1236–1243, 2014.

[105] F. Zhang, Y. Xia, L. Wang, L. Liu, Y. Liu, and J. Leng, “Conductive Shape Memory Microfiber Membranes with Core–Shell Structures and Electroactive Performance,” *ACS Appl. Mater. Interfaces*, vol. 10, no. 41, pp. 35526–35532, Oct. 2018.

[106] M. Bao, X. Lou, Q. Zhou, W. Dong, H. Yuan, and Y. Zhang, “Electrospun Biomimetic Fibrous Scaffold from Shape Memory Polymer of PDLLA-co-TMC for Bone Tissue Engineering,” *ACS Appl. Mater. Interfaces*, vol. 6, no. 4, pp. 2611–2621, 2014.

[107] Q. Zhao, J. Wang, H. Cui, H. Chen, Y. Wang, and X. Du, “Programmed Shape-Morphing Scaffolds Enabling Facile 3D Endothelialization,” *Adv. Funct. Mater.*, vol. 28, no. 29, p. 1801027, 2018.

[108] C. Wang, H. Yue, Q. Feng, B. Xu, L. Bian, and P. Shi, “Injectable Nanoreinforced Shape-Memory Hydrogel System for Regenerating Spinal Cord Tissue from Traumatic Injury,” *ACS Appl. Mater. Interfaces*, vol. 10, no. 35, pp. 29299–29307, 2018.

[109] Q. Zhang, K. Kratz, and A. Lendlein, “Shape-memory properties of degradable electrospun scaffolds based on hollow microfibers,” *Polym. Adv. Technol.*, vol. 26, no. 12, pp. 1468–1475, 2015.

[110] A. Shirole, J. Sapkota, E. J. Foster, and C. Weder, “Shape Memory Composites Based on Electrospun Poly(vinyl alcohol) Fibers and a Thermoplastic Polyether Block Amide Elastomer,” *ACS Appl. Mater. Interfaces*, vol. 8, no. 10, pp. 6701–6708, Mar. 2016.

[111] S. L. Buffington, B. M. Posnick, J. Paul, and P. T. Mather, “Ternary Polymeric Composites Exhibiting Bulk and Surface Quadruple-Shape Memory Properties,” *ChemPhysChem*, vol. 19, no. 16, pp. 2014–2024, 2018.

[112] H. Lu, Y. Yao, J. Yin, and L. Lin, “Functionally graded carbon nanotube and nafion/silica nanofibre for electrical actuation of carbon fibre reinforced shape memory polymer,” *Pigment Resin Technol.*, vol. 45, no. 2, pp. 93–98, Mar. 2016.

[113] Y. Yao, Y. Luo, H. Lu, and B. Wang, “Remotely actuated porous composite membrane with shape memory property,” *Compos. Struct.*, vol. 192, pp. 507–515, May 2018.

[114] E. D. Rodriguez, D. C. Weed, and P. T. Mather, “Anisotropic Shape-Memory Elastomeric Composites: Fabrication and Testing,” *Macromol. Chem. Phys.*, vol. 214, no. 11, pp. 1247–1257, 2013.

[115] H. Chen *et al.*, “Electrospun shape memory film with reversible fibrous structure,” *J. Mater. Chem.*, vol. 22, no. 42, pp. 22387–22391, 2012.

[116] H. Matsumoto *et al.*, “Shape-memory properties of electrospun non-woven fabrics prepared from degradable polyesterurethanes containing poly(ω-pentadecalactone) hard segments,” *Eur. Polym. J.*, vol. 48, no. 11, pp. 1866–1874, Nov. 2012.

[117] A. Iregui *et al.*, “Electrospinning of cationically polymerized epoxy/polycaprolactone blends to obtain shape memory fibers (SMF),” *Eur. Polym. J.*, vol. 94, pp. 376–383, Sep. 2017.

[118] X. Yan *et al.*, “Portable melt electrospinning apparatus without an extra electricity supply,” *RSC Adv.*, vol. 7, no. 53, pp. 33132–33136, 2017.

[119] L. Larrondo and R. S. J. Manley, “Electrostatic Fiber Spinning from Polymer Melts. I. Experimental Observations on Fiber Formation and Properties,” *J. Polym. Sci. Polym. Phys. Ed.*, vol. 19, no. 6, pp. 909–920, 1981.

[120] L. Larrondo and R. St. John Manley, “Electrostatic fiber spinning from polymer melts. II. Examination of the flow field in an electrically driven jet,” *J. Polym. Sci. Polym. Phys. Ed.*, vol. 19, no. 6, pp. 921–932, 1981.

[121] L. Larrondo and R. St. John Manley, “Electrostatic fiber spinning from polymer melts. III. Electrostatic deformation of a pendant drop of polymer melt,” *J. Polym. Sci. Polym. Phys. Ed.*, vol. 19, no. 6, pp. 933–940, 1981.

[122] D. W. Hutmacher and P. D. Dalton, “Melt electrospinning,” *Chem. - An Asian J.*, vol. 6, no. 1, pp. 44–56, 2011.

[123] C. S. Kong, K. J. Jo, N. K. Jo, and H. S. Kim, “Effects of the spin line temperature profile and melt index of poly(propylene) on melt-electrospinning,” *Polym. Eng. Sci.*, vol. 49, no. 2, pp. 391–396, Feb. 2009.

[124] N. Detta *et al.*, “Melt electrospinning of polycaprolactone and its blends with poly(ethylene glycol),” *Polym. Int.*, vol. 59, no. 11, pp. 1558–1562, Nov. 2010.

[125] M. Dasdemir, M. Topalbekiroglu, and A. Demir, “Electrospinning of thermoplastic polyurethane microfibers and nanofibers from polymer solution and melt,” *J. Appl. Polym. Sci.*, vol. 127, no. 3, pp. 1901–1908, Feb. 2013.

[126] F. Zhao, Y. Liu, H. Yuan, and W. Yang, “Orthogonal design study on factors affecting the degradation of polylactic acid fibers of melt electrospinning,” *J. Appl. Polym. Sci.*, vol. 125, no. 4, pp. 2652–2658, 2012.

[127] T. Jungst *et al.*, “Melt electrospinning onto cylinders: effects of rotational velocity and collector diameter on morphology of tubular structures,” *Polym. Int.*, vol. 64, no. 9, pp. 1086–1095, 2015.

[128] X. Li, Z. Wang, J. Wang, J. Liu, and C. Li, “Preparation and properties of TPU micro/nanofibers by a laser melt-electrospinning system,” *Polym. Eng. Sci.*, vol. 54, no. 6, pp. 1412–1417, 2014.

[129] A. Doustgani and E. Ahmadi, “Melt electrospinning process optimization of polylactic acid nanofibers,” *J. Ind. Text.*, vol. 45, no. 4, pp. 626–634, 2016.

[130] M. Dasdemir, G. S. Kozanoglu, M. Topalbekiroglu, and A. Demir, “Production and comparison of solution and melt electrospun thermoplastic polyurethane nanofibers,” in *Fiber Society 2007 Spring Conference - Advanced Polymer Fiber Materials Science and its Applications in Novel Engineered Products*, 2007, no. Fiber Soc. 2007 Spring Conf.-Adv. Polym. Fiber Mater. Sci. its Appl. Nov. Eng. Prod., pp. 74–76.

[131] G. Hochleitner *et al.*, “Additive manufacturing of scaffolds with sub-micron filaments via melt electrospinning writing,” *Biofabrication*, vol. 7, no. 3, p. 35002, 2015.

[132] A. Hrynevich *et al.*, “Dimension-Based Design of Melt Electrowritten Scaffolds,” *Small*, vol. 14, no. 22, p. 1800232, 2018.

[133] X. F. Wang and Z. M. Huang, “Melt-electrospinning of PMMA,” *Chinese J. Polym. Sci. (English Ed.*, vol. 28, no. 1, pp. 45–53, 2010.

[134] R. Deng, Y. Liu, Y. Ding, P. Xie, L. Luo, and W. Yang, “Melt electrospinning of low-density polyethylene having a low-melt flow index,” *J. Appl. Polym. Sci.*, vol. 114, no. 1, pp. 166–175, Oct. 2009.

[135] J. Lyons, C. Li, and F. Ko, “Melt-electrospinning part I: processing parameters and geometric properties,” *Polymer (Guildf).*, vol. 45, no. 22, pp. 7597–7603, 2004.

[136] Y. Kadomae, Y. Maruyama, M. Sugimoto, T. Taniguchi, and K. Koyama, “Relation between tacticity and fiber diameter in melt-electrospinning of polypropylene,” *Fibers Polym.*, vol. 10, no. 3, pp. 275–279, 2009.

[137] S. Tian, N. Ogata, N. Shimada, K. Nakane, T. Ogihara, and M. Yu, “Melt electrospinning from poly(L-lactide) rods coated with poly(ethylene-co-vinyl alcohol),” *J. Appl. Polym. Sci.*, vol. 113, no. 2, pp. 1282–1288, 2009.

[138] N. Ogata, N. Shimada, S. Yamaguchi, K. Nakane, and T. Ogihara, “Melt-electrospinning of poly(ethylene terephthalate) and polyalirate,” *J. Appl. Polym. Sci.*, vol. 105, no. 3, pp. 1127–1132, 2007.

[139] P. D. Dalton, J. Lleixà Calvet, A. Mourran, D. Klee, and M. Möller, “Melt electrospinning of poly-(ethylene glycol-block-ϵ-caprolactone),” *Biotechnol. J.*, vol. 1, no. 9, pp. 998–1006, 2006.

[140] N. Ogata, G. Lu, T. Iwata, S. Yamaguchi, K. Nakane, and T. Ogihara, “Effects of ethylene content of poly(ethylene-co-vinyl alcohol) on diameter of fibers produced by melt-electrospinning,” *J. Appl. Polym. Sci.*, vol. 104, no. 2, pp. 1368–1375, 2007.

[141] F. M. Wunner *et al.*, “Melt Electrospinning Writing of Highly Ordered Large Volume Scaffold Architectures,” *Adv. Mater.*, vol. 30, no. 20, p. 1706570, May 2018.

[142] M. L. Muerza-Cascante *et al.*, “Endosteal-like extracellular matrix expression on melt electrospun written scaffolds,” *Acta Biomater.*, vol. 52, pp. 145–158, Apr. 2017.

[143] T. D. Brown *et al.*, “Design and Fabrication of Tubular Scaffolds via Direct Writing in a Melt Electrospinning Mode,” *Biointerphases*, vol. 7, no. 1, p. 13, 2012.

[144] S. J. Kim, D. H. Jang, W. H. Park, and B. M. Min, “Fabrication and characterization of 3-dimensional PLGA nanofiber/microfiber composite scaffolds,” *Polymer (Guildf).*, vol. 51, no. 6, pp. 1320–1327, 2010.

[145] A. Karchin, F. I. Simonovsky, B. D. Ratner, and J. E. Sanders, “Melt electrospinning of biodegradable polyurethane scaffolds,” *Acta Biomater.*, vol. 7, no. 9, pp. 3277–3284, 2011.

[146] P. D. Dalton, N. T. Joergensen, J. Groll, and M. Moeller, “Patterned melt electrospun substrates for tissue engineering.,” *Biomed. Mater.*, vol. 3, no. 3, p. 034109, 2008.

[147] S. Lee and S. K. Obendorf, “Developing protective textile materials as barriers to liquid penetration using melt-electrospinning,” *J. Appl. Polym. Sci.*, vol. 102, no. 4, pp. 3430–3437, 2006.

[148] E. McColl, J. Groll, T. Jungst, and P. D. Dalton, “Design and fabrication of melt electrowritten tubes using intuitive software,” *Mater. Des.*, vol. 155, pp. 46–58, Oct. 2018.

[149] G. Hochleitner, E. Fürsattel, R. Giesa, J. Groll, H.-W. Schmidt, and P. D. Dalton, “Melt Electrowriting of Thermoplastic Elastomers,” *Macromol. Rapid Commun.*, vol. 39, no. 10, p. 1800055, 2018.

[150] G. Hochleitner, F. Chen, C. Blum, P. D. Dalton, B. Amsden, and J. Groll, “Melt electrowriting below the critical translation speed to fabricate crimped elastomer scaffolds with non-linear extension behaviour mimicking that of ligaments and tendons,” *Acta Biomater.*, vol. 72, pp. 110–120, May 2018.

[151] T. D. Brown, P. D. Dalton, and D. W. Hutmacher, “Direct Writing By Way of Melt Electrospinning,” *Adv. Mater.*, vol. 23, no. 47, pp. 5651–5657, 2011.

[152] T. D. Brown, P. D. Dalton, and D. W. Hutmacher, “Melt electrospinning today: An opportune time for an emerging polymer process,” *Prog. Polym. Sci.*, vol. 56, pp. 116–166, May 2016.

[153] S. B. Mitchell and J. E. Sanders, “A unique device for controlled electrospinning,” *J. Biomed. Mater. Res. Part A*, vol. 78A, no. 1, pp. 110–120, 2006.

[154] C. Hacker, Z. Karahaliloglu, G. Seide, E. B. Denkbas, and T. Gries, “Functionally modified, melt-electrospun thermoplastic polyurethane mats for wound-dressing applications,” *J. Appl. Polym. Sci.*, vol. 131, no. 8, 2014.

[155] R. Nayak, R. Padhye, I. L. Kyratzis, Y. B. Truong, and L. Arnold, “Effect of viscosity and electrical conductivity on the morphology and fiber diameter in melt electrospinning of polypropylene,” *Text. Res. J.* , vol. 83, no. 6, pp. 606–617, Apr. 2013.

[156] Y. Shen, Q. Liu, B. Deng, P. Yao, and S. Xia, “Experimental study and prediction of the diameter of melt-electrospinning polypropylene fiber,” *Fibers Polym.*, vol. 17, no. 8, pp. 1227–1237, 2016.

[157] P. D. Dalton, D. Grafahrend, K. Klinkhammer, D. Klee, and M. Möller, “Electrospinning of polymer melts: Phenomenological observations,” *Polymer (Guildf).*, vol. 48, no. 23, pp. 6823–6833, Nov. 2007.

[158] E. Zhmayev, D. Cho, and Y. L. Joo, “Electrohydrodynamic quenching in polymer melt electrospinning,” *Phys. Fluids*, vol. 23, no. 7, p. 73102, 2011.

[159] X. Li, H. Liu, J. Wang, and C. Li, “Preparation and characterization of poly(ε-caprolactone) nonwoven mats via melt electrospinning,” *Polymer (Guildf).*, vol. 53, no. 1, pp. 248–253, 2012.

[160] G. Hochleitner *et al.*, “Fibre pulsing during melt electrospinning writing,” *BioNanoMaterials*, vol. 17, no. 3–4, pp. 159–171, 2016.

[161] H. Zhou, T. B. Green, and Y. L. Joo, “The thermal effects on electrospinning of polylactic acid melts,” *Polymer (Guildf).*, vol. 47, no. 21, pp. 7497–7505, 2006.

[162] H. Zhou, “ELECTROSPUN FIBERS FROM BOTH SOLUTION AND MELT: PROCESSING, STRUCTURE AND PROPERTY,” Cornell University, 2007.

[163] E. Zhmayev, D. Cho, and Y. L. Joo, “Nanofibers from gas-assisted polymer melt electrospinning,” *Polymer (Guildf).*, vol. 51, no. 18, pp. 4140–4144, 2010.

[164] P. D. Dalton, K. Klinkhammer, J. Salber, D. Klee, and M. Möller, “Direct in vitro electrospinning with polymer melts,” *Biomacromolecules*, vol. 7, no. 3, pp. 686–690, 2006.

[165] S. N. Malakhov *et al.*, “Method of manufacturing Nonwovens by electrospinning from polymer melts,” *Fibre Chem.*, vol. 41, no. 6, pp. 355–359, 2009.

[166] Z. K. Nagy *et al.*, “Solvent-free melt electrospinning for preparation of fast dissolving drug delivery system and comparison with solvent-based electrospun and melt extruded systems,” *J. Pharm. Sci.*, vol. 102, no. 2, pp. 508–517, 2013.

[167] Y. Weimin and L. Haoyi, “Principle and equipment of polymer melt differential electrospinning preparing ultrafine fiber,” *IOP Conf. Ser. Mater. Sci. Eng.*, vol. 64, no. 1, p. 12013, 2014.

[168] F. Chen, G. Hochleitner, T. Woodfield, J. Groll, P. D. Dalton, and B. G. Amsden, “Additive Manufacturing of a Photo-Cross-Linkable Polymer via Direct Melt Electrospinning Writing for Producing High Strength Structures,” *Biomacromolecules*, vol. 17, no. 1, pp. 208–214, 2016.

[169] H. Rajabinejad, R. Khajavi, A. Rashidi, N. Mansouri, and M. E. Yazdanshenas, “Recycling of used bottle grade poly ethyleneterephthalate to nanofibers by melt-electrospinning method,” *Int. J. Environ. Res.*, vol. 3, no. 4, pp. 663–670, 2009.

[170] E. Zhmayev, D. Cho, and Y. L. Joo, “Modeling of melt electrospinning for semi-crystalline polymers,” *Polymer (Guildf).*, vol. 51, no. 1, pp. 274–290, 2010.

[171] E. Zhmayev, H. Zhou, and Y. L. Joo, “Modeling of non-isothermal polymer jets in melt electrospinning,” *J. Nonnewton. Fluid Mech.*, vol. 153, no. 2–3, pp. 95–108, 2008.

[172] N. Shimada, H. Tsutsumi, K. Nakane, T. Ogihara, and N. Ogata, “Poly(ethylene-co-vinyl alcohol) and Nylon 6/12 nanofibers produced by melt electrospinning system equipped with a line-like laser beam melting device,” *J. Appl. Polym. Sci.*, vol. 116, no. 5, pp. 2998–3004, 2010.

[173] SMP Technologies Inc., “SHAPE MEMORY POLYMER.” [Online]. Available: http://www2.smptechno.com/en/smp/. [Accessed: 2019].

[174] "Download Marlin." [Online]. Available: https://marlinfw.org/meta/download/. [Accessed: 2019].

[175] M. L. Rivera and S. E. Hudson, "Desktop Electrospinning: A Single Extruder 3D Printer for Producing Rigid Plastic and Electrospun Textiles," in *Proceedings of the 2019 CHI Conference on Human Factors in Computing Systems*, 2019, pp. 1–12.

[176] Gamma High Voltage Reaserach, "Series ES." [Online]. Available: http://www.gammahighvoltage.com/html/series_es.html. [Accessed: 2019].

[177] C. A. Schneider, W. S. Rasband, and K. W. Eliceiri, "NIH Image to ImageJ: 25 years of image analysis," *Nat. Methods*, vol. 9, no. 7, pp. 671–675, Jul. 2012.

[178] F. K. Ko and Y. Wan, "Characterization of nanofibers," in *Introduction to Nanofiber Materials*, Cambridge University Press, 2014, pp. 101–145.

[179] L.-H. Zhang *et al.*, "Recent advances in melt electrospinning," *RSC Adv.*, vol. 6, no. 58, pp. 53400–53414, 2016.

[180] C. C. Qin *et al.*, "Melt electrospinning of poly(lactic acid) and polycaprolactone microfibers by using a hand-operated Wimshurst generator," *Nanoscale*, vol. 7, no. 40, pp. 16611–16615, 2015.

[181] K. H. Lee, H. Y. Kim, Y. J. Ryu, K. W. Kim, and S. W. Choi, "Mechanical behavior of electrospun fiber mats of poly(vinyl chloride)/polyurethane polyblends," *J. Polym. Sci. Part B Polym. Phys.*, vol. 41, no. 11, pp. 1256–1262, 2003.

[182] I. Greenfeld, X. Sui, and H. D. Wagner, "Stiffness, Strength, and Toughness of Electrospun Nanofibers: Effect of Flow-Induced Molecular Orientation," *Macromolecules*, vol. 49, no. 17, pp. 6518–6530, 2016.

[183] A. Nissenbaum, I. Greenfeld, and H. D. Wagner, "Shape memory polyurethane - Amorphous molecular mechanism during fixation and recovery," *Polymer (Guildf).*, vol. 190, p. 122226, 2020.

[184] A. Leonés, A. Sonseca, D. López, S. Fiori, and L. Peponi, “Shape memory effect on electrospun PLA-based fibers tailoring their thermal response,” *Eur. Polym. J.*, vol. 117, no. May, pp. 217–226, 2019.

[185] J. Kaursoin and A. K. Agrawal, “Melt spun thermoresponsive shape memory fibers based on polyurethanes: Effect of drawing and heat-setting on fiber morphology and properties,” *J. Appl. Polym. Sci.*, vol. 103, no. 4, pp. 2172–2182, 2007.